Imprinted SARS-CoV-2 humoral immunity induces convergent Omicron RBD evolution

Yunlong Cao[1,2,#,*], Fanchong Jian[1,3,#], Jing Wang[1,4,#], Yuanling Yu[2,#], Weiliang Song[1,4], Ayijiang Yisimayi[1,4], Jing Wang[2], Ran An[2], Na Zhang[2], Yao Wang[2], Peng Wang[2], Lijuan Zhao[2], Haiyan Sun[2], Lingling Yu[2], Sijie Yang[1,5], Xiao Niu[1,3], Tianhe Xiao[1,6], Qingqing Gu[2], Fei Shao[2], Xiaohua Hao[7], Yanli Xu[7], Ronghua Jin[7], Youchun Wang[2,8,*], Xiaoliang Sunney Xie[1,2,*]

[1]Biomedical Pioneering Innovation Center (BIOPIC), Peking University, Beijing, P.R. China.

[2]Changping Laboratory, Beijing, P.R. China.

[3]College of Chemistry and Molecular Engineering, Peking University, Beijing, P.R. China.

[4]School of Life Sciences, Peking University, Beijing, P.R. China.

[5]Peking-Tsinghua Center for Life Sciences, Peking University, Beijing, P.R. China.

[6]Joint Graduate Program of Peking-Tsinghua-NIBS, Academy for Advanced Interdisciplinary Studies, Peking University, Beijing, China.

[7]Beijing Ditan Hospital, Capital Medical University, Beijing, P.R. China.

[8]Division of HIV/AIDS and Sex-transmitted Virus Vaccines, Institute for Biological Product Control, National Institutes for Food and Drug Control (NIFDC), Beijing, P.R. China.

[*]Correspondence: Youchun Wang (wangyc@nifdc.org.cn); Xiaoliang Sunney Xie (sunneyxie@biopic.pku.edu.cn); Yunlong Cao (yunlongcao@pku.edu.cn).

[#]These authors contributed equally.

Abstract

Continuous evolution of Omicron has led to numerous subvariants that exhibits growth advantage over BA.5. Such rapid and simultaneous emergence of variants with enormous advantages is unprecedented. Despite their rapidly divergent evolutionary courses, mutations on their receptor-binding domain (RBD) converge on several hotspots, including R346, R356, K444, L452, N460K and F486. The driving force and destination of such convergent evolution and its impact on humoral immunity established by vaccination and infection remain unclear. Here we demonstrate that these convergent mutations can cause striking evasion of convalescent plasma, including those from BA.5 breakthrough infection, and existing antibody drugs, including Evusheld and Bebtelovimab. BA.2.75.2 is the most evasive strain tested, and only BQ.1.1 could compare. To clarify the origin of the convergent evolution, we determined the escape mutation profiles and neutralization activity of monoclonal antibodies (mAbs) isolated from convalescents of BA.2 and BA.5 breakthrough infection. Importantly, due to humoral immune imprinting, BA.2 and especially BA.5 breakthrough infection caused significant reductions of neutralizing antibody epitope diversity and increased proportion of non-neutralizing mAbs, which in turn concentrated humoral immune pressure and promoted the convergent RBD evolution. Additionally, the precise convergent RBD mutations and evolution trends of BA.2.75/BA.5 subvariants could be inferred by integrating the neutralization-weighted DMS profiles of mAbs from various immune histories (3051 mAbs in total). Moreover, we demonstrated that as few as five additional convergent mutations based on BA.5 or BA.2.75 could completely evade most plasma samples, including those from BA.5 breakthrough infections, while remaining sufficient hACE2-binding affinity. These results suggest herd immunity established by natural infection could hardly stop RBD evolution, and vaccine boosters using BA.5 may not provide sufficiently broad protection. Broad-spectrum SARS-CoV-2 vaccines and NAb drugs development should be in high priority and the constructed convergent mutants could serve to examine their effectiveness in advance.

Main

SARS-CoV-2 Omicron BA.1, BA.2 and BA.5 have demonstrated strong neutralization evasion capability, posing severe challenges to the efficacy of existing humoral immunity established through vaccination and infection [1-15]. Nevertheless, Omicron is continuously evolving, leading to various new subvariants, including BA.2.75 and BA.4.6 [16-22]. Importantly, a high proportion of these emerging variants displayed high growth advantages over BA.5, such as BA.2.3.20, BA.2.75.2, BR.1, BN.1, BJ.1 and BQ.1.1 (Fig. 1a) [23]. Such rapid and simultaneous emergence of multiple variants with enormous growth advantages is unprecedented. Notably, although these derivative subvariants appear to diverge along the evolutionary course, the mutations they carry on the receptor-binding domain (RBD) converge on the same sites, including R346, K444, V445, G446, N450, L452, N460, F486, F490, and R493 (Fig. 1b). Most mutations on these residues are known to be antibody-evasive, as revealed by deep mutational scanning (DMS) [1,2,24-26]. It's crucial to examine the impact of these convergent mutations on antibody-escaping capability, receptor binding affinity, and the efficacy of vaccines and antibody therapeutics. It's also important to investigate the driving force behind this accelerated RBD mutation, what such mutational convergence would lead to, and how we can prepare for such convergent RBD evolution.

Convergent RBD evolution causes further immune evasion

First, we tested the antibody evasion capability of these variants. We constructed the VSV-based spike-pseudotyped virus of Omicron BA.2, BA.2.75 and BA.4/5 lineages carrying those convergent mutations and examined the neutralizing activities of therapeutic neutralizing antibodies (NAbs) against them [13,27-32]. The COV2-2196+COV2-2130 (Evusheld) [28,33] are vulnerable to F486, R346, and K444 mutations, evaded or highly impaired by BA.2.38.1 (K444N), BJ.1 (R346T), BR.1 (L452R+K444M), BA.5.2.7 (K444M), BA.5.6.2 (K444T). LY-CoV1404 (Bebtelovimab) remains potent against BF.16 (K444R), BA.5.1.12 (V445A), and shows reduced potency against BA.5.5.1 (N450D) [31]. However, LY-CoV1404 was escaped by BJ.1 and BR.1, and exhibited strongly reduced activity against BA.2.38.1, BA.5.2.7 and BA.5.6.2 due to K444 N/M/T mutations [31]. SA55+SA58 is a pair of broad NAbs isolated from

vaccinated SARS convalescents and targeting non-competing conserved epitopes [2,32]. Here SA55 demonstrated high potency against all tested Omicron subvariants, although SA58 was evaded by BA.2.77, and showed reduced neutralization efficacy against BJ.1 and some of the BA.2.75 variants (Fig. 2a). However, SA55+SA58 are still in preclinical developmental stage and expected to start its Phase 1 clinical trial in early 2023. This means the efficacy of available antibody drugs, including BA.2.75/BA.5-effective Evusheld and Bebtelovimab, are strongly affected by the emerging subvariants with convergent mutations.

To gain an advantage in transmissibility, sufficient ACE2-binding affinity is essential. We examined the relative hACE2 binding affinity of these variants by evaluating hACE2 neutralizing potency against pseudoviruses. Higher neutralizing efficacy of ACE2 indicates a higher binding affinity of the variant [18]. Overall, these variants demonstrate sufficient ACE2-binding affinity, at least higher than D614G, allowing their prevalence (Fig. 2b). Specifically, R493Q reversion increased the binding affinity to hACE2, which is consistent with previous reports [4,18,20]. K417T shows a moderate increase in binding affinity to hACE2. In contrast, F486S, K444M, K444N have negative impact on binding affinity, while K444T does not cause significant impairment on ACE2 binding (Fig. 2b). These observations are also in line with previous DMS results [34].

In addition, we investigated how these variants escape the neutralization of plasma samples from individuals with various immune history. We recruited cohorts of individuals who received 3 doses of CoronaVac [35] with or without breakthrough infection by BA.1, BA.2, or BA.5. Convalescent plasma samples were collected around 4 weeks after the discharge from hospital (Supplementary Table 1). Plasma from CoronaVac vaccinees were obtained two weeks after the third dose. Compared to the NT50 against BA.2, significant reduction in NT50 against all tested BA.2 subvariants are observed (Fig. 2c-f). BJ.1 which carries 7 additional RBD mutations compared to BA.2 is highly immune evasive; however, newly emerging BA.2.75 and BA.5 subvariants demonstrated even stronger antibody-evading capability. BA.5 subvariants with R346T, K444T/R and V445A exhibited similar reduction in NT50, while N450D is slightly less evasive than others. Among all tested strains, BA.2.75.2 (R346T+F486S) is the most evasive, causing a reduction in NT50 of plasma from 3-dose vaccinees, BA.1

breakthrough infection, BA.2 breakthrough infection and BA.5 breakthrough infection by 4.2, 5.9, 6.2 and 2.7-fold compared to BA.2.75, respectively. BR.1, which carries L452R+K444M compared to BA.2.75, further reduces the NT50 of plasma from 3-dose vaccinees, BA.1, BA.2 and BA.5 breakthrough infection by 3.1, 2.3, 3.5 and 1.7 folds, respectively. These observations demonstrate that convergent RBD evolution could cause significant immune escape at a scale never seen before. Such rapid and convergent emergence of antibody-escaping variants, especially their capability of evading convalescent plasma from BA.5 breakthrough infection, suggest that vaccine boosters designed based on BA.5 may not achieve broad-spectrum effectiveness.

Immune imprinting induces convergent RBD evolution

It is crucial to investigate the origin of such accelerated RBD convergent evolution with increasing growth advantage. Therefore, we characterized the antibody repertoires induced by Omicron BA.2 and BA.5 breakthrough infection, which is the dominant immune background of current global herd immunity. As the strategy described in our previous report using PBMC from BA.1 breakthrough infection [2], we enriched antigen-specific memory B cells by fluorescence-activated cell sorting (FACS) for individuals who had recovered from BA.2 and BA.5 breakthrough infection. RBD-binding $CD27^+$ IgM/IgD^- cells were subjected to single-cell V(D)J sequencing (scVDJ-seq) to determine the BCR sequences.

Similar to that reported in BA.1 breakthrough infection, the phenomenon of immune imprinting, or so-called "original antigenic sin", is also observed in BA.2 and BA.5 breakthrough infection [2,36-39]. Post-vaccination infection with BA.2 and BA.5 mainly recalls cross-reactive memory B cells elicited by wild type-based vaccine, but rarely produces BA.2/BA.5 specific B cells, similar to BA.1 breakthrough infection. About 68.6% of the BA.5 RBD binding B cells from BA.5 infection also bind to WT RBD (Fig 3a). Likewise, around 70.1% of the BA.2 RBD binding B cells from post-vaccination BA.2 infection can cross bind to WT RBD, compared to 19.7% for BA.2 infection without vaccination (Fig 3b, 3c). The RBD-targeting antibody sequences determined by scVDJ-seq are then expressed *in vitro* as human IgG1 monoclonal antibodies (mAbs). Among the expressed mAbs, only a small proportion specifically binds to

BA.2/BA.5 RBD and is not cross-reactive to WT RBD, determined by enzyme-linked immunosorbent assay (ELISA), which is concordant with the FACS results (Fig. 3d). Importantly, cross-reactive mAbs exhibited significantly higher somatic hypermutation (SHM), indicating that these antibodies are more affinity-matured and are most likely recalled from previously vaccination-induced memory (Fig. 3d).

Next, we determined the escaping mutation profiles of these antibodies by high-throughput DMS and measured their neutralizing activities against SARS-CoV-2 D614G, BA.2, BA.5 and BA.2.75 (Fig. 3e, Extended Data Fig. 2a-b). Previously, we reported the DMS profiles and the epitope distribution of antibodies isolated from WT vaccinated/infected individuals, SARS-CoV-2 vaccinated SARS convalescents, and BA.1 convalescents, which could be classified into 12 epitope groups [2]. Among them, mAbs in groups A, B, C, D1, D2, F2 and F3 compete with ACE2 and exhibit neutralizing activity; while mAbs in E1, E2.1, E2.2, E3 and F1 does not compete with ACE2, among which E2.2, E3 and F1 exhibit low or no neutralizing capability. To integrate the DMS profiles of the new mAbs isolated from BA.2 and BA.5 convalescents with previous dataset, we co-embedded all antibodies using multidimensional scaling (MDS) based on their DMS profiles, followed by *t*-distributed stochastic neighbor embedding (*t*-SNE) for visualization, and used KNN-based classification to determine the epitope groups of new mAbs (Fig. 3e). This results in a dataset containing the DMS profiles of 3051 SARS-CoV-2 WT RBD-targeting mAbs. The epitope distribution of mAbs from BA.2 breakthrough infection is generally similar to those elicited by BA.1, except for the increased proportion of mAbs in group C. However, BA.5-elicited mAbs showed more distinct distribution compared to BA.1, with significantly increased proportion of mAbs in group D2 and E2.2, and decreased ratio of antibodies in groups B and E2.1. The main reason is that, the immune evasion caused by F486 and L452 mutations makes these cross-reactive memory B cells unable to be activated (Fig. 3f, Extended Data Fig. 3b and 5a). Remarkably, repertoires induced by all Omicron breakthrough infection are distinct to those stimulated by WT. Compared to WT infection or vaccination, BA.1, BA.2 and BA.5 breakthrough infection mainly elicit mAbs of group E2.2, E3 and F1, which do not compete with ACE2 and demonstrate weak neutralizing activity, while WT-elicited antibodies enrich ACE2-competing

groups A-C with strong neutralization (Fig. 3g-h and Extended Data Fig. 3a-c). Strikingly, the combined proportion of E2.2, E3, and F1 antibodies rise from 29% in WT convalescents/vaccinees, 53% in BA.1 convalescents, 51% in BA.2 convalescents, to 63% in BA.5 convalescents (Fig. 3f). Overall, the proportion and diversity of neutralizing antibody epitopes are reduced in Omicron breakthrough infection, with BA.5 displaying the most severe. Our results demonstrate post-vaccination infection with Omicron variants, including BA.1, BA.2, and BA.5, mainly recalls cross-reactive memory B cells elicited by WT-based vaccines, instead of producing a larger proportion of Omicron-specific B cells. Such immune imprinting reduces the NAb epitope diversity and causes increased proportion of E2.2, E3, and F1 antibodies which exhibit weak or no neutralization.

To clarify the impact of the immune imprinting and consequent reduction of NAb epitope diversity on the RBD evolutionary pressure caused by humoral immunity, we aggregated DMS profiles of multiple mAbs to estimate the impact of mutations on the efficacy of polyclonal antibodies, which is inspired by a previous work (Supplementary Table 2) [40]. It is essential to incorporate the effects of ACE2 binding, RBD expression, neutralizing activity of mAbs, and the constraint of codon usage to archive a reasonable estimation. In brief, each mutation on the RBD would have an impact on each mAb in the set, which is quantified by the escape scores determined by DMS and will be weighted by its IC50 against the evolving strain, as the pressure of an antibody is negatively correlated with the neutralizing activity. For each residue, only those amino acids that are accessible by one nucleotide mutation are included. Impacts on ACE2-binding affinity and RBD expression of each mutation are also considered in the analyses, using data determined by DMS in previous reports [34,41,42]. Finally, the estimated relative preference of each mutation is calculated using the sum of weighted escape scores of all mAbs in the specific set, considering all factors mentioned above, including neutralizing activity, codon usage, ACE2-binding affinity, and RBD expression.

The reduced NAb epitope diversity caused by imprinted humoral response could be strikingly shown by the estimated preference spectrum, given that there are diversified peaks while using BA.2-elicited antibodies with IC50 against BA.2 for calculation, but only two major peaks, R346T/S and K444E/Q/N/T/M, could be identified using BA.5-elicited antibodies with IC50

against BA.5 (Fig. 4a). Interestingly, these two hotspots are two of the most frequently mutated sites in continuously evolving BA.4/5 subvariants, and convergently occur in multiple lineages (Fig. 1a-b and Extended Data Fig. 1). Similar analysis for WT and BA.1 also demonstrated various peaks (Extended Data Fig. 6a-b). Thus, the concentrated immune pressure strikingly reflects the reduced diversity of NAbs elicited by BA.5 breakthrough infection due to immune imprinting, and these concentrated preferred mutations are highly overlapped with observed convergent hotspots in the real world. Together, our results indicate that the convergent RBD evolution is promoted by imprinted humoral response.

Accurate inference of RBD evolution hotspots

Moreover, we wonder if the real-world evolution trends of SARS-CoV-2 RBD could be rationalized and even predicted by aggregating this large DMS dataset containing mAbs from various immune histories. Using the mAbs from vaccinated or convalescent individuals from WT with IC50 against D614G strain, we find mutations with highest scores include K417N/T, K444-G446, N450, L452R, and especially E484K (Extended Data Fig. 6a). Most of these residues were mutated in previous VOCs, such as K417N/E484K in Beta, K417T/E484K in Gamma, L452R in Delta, and G446S/E484A in Omicron BA.1, confirming the reasonableness of our estimation and inference. Evidence on the emergence of BA.2.75 and BA.5 could be found using WT, BA.1, and BA.2-elicited mAbs with IC50 against BA.2, where peaks on 444-446, 452, 460, and 486 could be identified (Extended Data Fig. 6c). To better investigate the evolution trends of BA.2.75 and BA.5, two main lineages circulating currently, considering a large part of the world population are still in the antibody environment constructed by WT-based vaccination, we then included antibodies elicited by previous strains in the dataset, with IC50 against BA.2.75 or BA.5 for calculation (Fig. 4b and Extended Data Fig. 6d). For BA.2.75, the most significant sites are R346T/S, K356T, N417Y/H/I/T, K444E/Q/N/T/M, V445D/G/A, N450T/D/K/S, L452R, I468N, A484P, F486S/V, and F490S/Y. We noticed that these identified residues, even most specific mutations, are highly overlapped with recent mutation hotspots of BA.2.75 (Fig. 1b). An exception is A484/F490, which is feature residues of Group C and could be covered by L452R (Extended Data Fig. 3d). I468 is also highly associated with K356 (Extended Data Fig. 5b-c). Due to the stronger antibody evasion of BA.5, the preference

spectrum of BA.5 is much more concentrated compared to BA.2.75, but the remaining sites are highly overlapped and complementary with BA.2.75. The most striking residues are R346, K444-G446, and N450, followed by K356, N417, L455, N460 and A484. As expected, L452R/F486V that have appeared in BA.5 disappeared in the preference spectrum, while N460K harbored by BA.2.75 appears. These sites and mutations are also popular in emerging BA.4/5 subvariants.

Convergent evolution could eventually nullify plasma neutralization

To further examine the antibody-escaping capabilities of mutations on the identified convergent hotspots. We selected a panel of 178 NAbs from 8 epitope groups that could potently neutralize BA.2, and determined their neutralizing activity against constructed mutants carrying single or combined convergent mutations (Fig. 4c and Extended Data Fig. 7). NABs from C and F1-F3 epitope groups were not included since they are either completely escaped by BA.2 or too rare in Omicron infected convalescents (Fig. 2f and Extended Data Fig. 3c-d). As expected, R493Q and N417T does not contribute a lot to antibody evasion, but R493Q significantly benefits ACE2 binding. Most group A NAbs are sensitive to N460K, and BA.5+N460K escapes the majority of NAbs in group A, because of the combination of F486V and N460K. All NAbs in group B are escaped by F486S/V, and G446S affects some of D1/D2 NAbs, as previously reported (Extended Data Fig. 3a-b) [20]. D1/D2 NAbs are more susceptible to K444N/T and N450D, and some D1 NAbs could also be escaped by L452R (Extended Data Fig. 4a-b). E1 is mainly affected by R346T, but minor evasion is also observed for D339H and K356T (Extended Data Fig. 4c). E2.1 and E2.2 exhibit similar properties, evaded by K356T and L452R. E3 antibodies seem not significantly affected by all constructed mutants as expected (Extended Data Fig. 5a-b), but they generally exhibit very low neutralization (Extended Data Fig. 5c-d and 7a). BA.5+R346T escapes most antibodies in D1, E1 and E2.1/E2.2, and an additional K444N further escapes most mAbs in D2, demonstrating the feasibility and effectiveness of combining convergent mutations to archive further evasion. All tested mutants including those carrying 6 mutations display sufficient hACE2-binding affinity, despite the reduced capability caused by K444N and F486S/V, which is also consistent with DMS [34,41]. These findings indicate the feasibility to generate a mutant harboring accumulated convergent escape

mutations without much compromise on hACE2-binding affinity. Interestingly, we observed several survivors that could broadly neutralize all tested mutants, which may be good candidates for clinical use (Fig. 4c and Extended Data Fig. 7a).

Although due to immune imprinting, the proportion of Omicron-specific mAbs are low, it is still necessary to evaluate their neutralization potency and breadth, especially against the convergent mutants. We tested the neutralizing activity of a panel of Omicron-specific RBD-targeting mAbs against D614G, BA.1, BA.2, BA.5, BA.2.75, BA.2.75.2, in addition to BA.5+R346T and BA.5+K444T, which are two important convergent RBD mutants. These mAbs were isolated from convalescent plasma with Omicron breakthrough infection (Fig. 4d). They could bind RBD of the corresponding eliciting Omicron variant, but do not cross-bind WT RBD, as confirmed by ELISA. We found these mAbs could effectively neutralize against the eliciting strain as expected, but exhibited poor neutralizing breadth, which means their potency would be largely impaired by other Omicron subvariants, consistent with our previous discovery and relatively low SHM rate [2]. Thus, these Omicron-specific antibodies would not effectively expand the breadth of the antibody repertoire of Omicron breakthrough infection.

We then evaluated the potency of NTD-targeting NAbs against BA.2.75, BA.5 and BA.2 with selected NTD mutations using a panel of 14 mAbs, as it is reported that NTD-targeting antibodies are abundant in plasma from BA.2 breakthrough infection[43]. The selected mutations are most from BA.2.75, except for R237T which was designed to escape mAbs targeting a certain epitope reported recently [20]. None of them exhibit strong neutralizing potency, and the IC50 values are all over 0.3 μg/mL [44,45] (Fig. 4e and Extended Data Fig. 7b). Regarding the five NTD mutations harbored by BA.2.75, we found W152R and K147E strikingly escapes similar NTD-targeting mAbs, F157L exhibited less evasive, while I210V and G257S did not significantly affect any tested mAbs, consistent with previous neutralization data using sera [18]. R237T escapes another group of NTD-targeting mAbs, which is distinct from the K147E/W152R-sensitive group [20].

Based on the observed and predicted the convergent hotpots on RBD, we wonder if we could construct the final result of the convergent RBD evolution and check to what extent it will

evade humoral immune response. Therefore, we designed multiple VSV-based pseudoviruses that gradually gain additional convergent mutations one by one (Fig. 5a). The constructed final mutant contains 11 additional mutations on the NTD and RBD compared to BA.5, or 9 mutations compared to BA.2.75. The neutralizing activities of Omicron-effective NAb drugs were first evaluated. As expected, majority of existing effective NAb-based drugs are escaped by these mutants, and the mutations that caused the evasion have also been discussed in previous sections. No residue on the SA55 epitope appeared in either real-world observation or DMS-based prediction of convergent hotspots, so it is reasonable that neutralization of SA55, or SA55+SA58 is not affected (Fig. 5b). Similarly, we also determined the ACE2-binding capability of these mutants by neutralization assays using hACE2 (Fig. 5c). Although some of the designed pseudoviruses exhibit reduced activity to hACE2 compared to original BA.2.75 or BA.5 variants, especially those with K444N and F486V, but the affinities of them are still higher than that of D614G (Fig. 2b). Importantly, our designed pseudoviruses could largely evade the plasma of vaccinees and convalescents after BA.1 breakthrough infection, BA.2 breakthrough infection, and even BA.5 breakthrough infection, which would greatly challenge the current herd immunity established through vaccination and infection (Fig. 5d-5g). Among the derivative mutants of BA.2.75, L452R, K444M, R346T, and F486V contribute to significant reduction in succession (Fig. 5d-f), except for plasma of BA.5 convalescents in which L452R does not cause further evasion, which is reasonable as L452R has appeared in BA.5 and antibodies that are not susceptible to L452R were elicited in these convalescents (Fig. 5g). More NTD mutations does not contribute to stronger evasion in BA.2.75-based mutants, but we observed significant reduction in NT50 of BA.2/BA.5 convalescents against BA.5-based mutants with K147E+W152R, suggesting BA.2/BA.5 convalescent plasma contains large proportion of NTD-targeting antibodies [43]. As the NTD of BA.1 is quite different from that of BA.2 and BA.5, we did not observe significant effects of NTD mutations on the efficacy of BA.1 convalescent plasma. Plasma neutralization titers of all the vaccinees and convalescents decreased to the lowest detection limit against BA.2.75 with 5 extra RBD mutations L452R, K444M, R346T, F486V and K356T, as the same for vaccinees or BA.1 convalescents against BA.5 with 4 extra RBD mutations K444N, R346T, N460K and K356T. The plasma from BA.2/BA.5 convalescents can tolerate more mutations based on BA.5, and

extra NTD mutations are needed, such as K147E and W152R, to completely eliminate their neutralization. Together, we demonstrated that as few as five additional mutations on BA.5 or BA.2.75 could completely evade most plasma samples, including those from BA.5 breakthrough infections, while remaining sufficient hACE2-binding affinity. Similar efforts have been made in a recent report despite different construction strategies [46]. The constructed evasive mutants, such as BA.2.75-S5/6/7/8 and BA.5-S7/8, could serve to examine the effectiveness of broad-spectrum vaccines and NAbs in advance.

In this work, we observed that convergent RBD evolution causes severe immune evasion, and could be rationalized and explained by integration of DMS profiles. Given the existence of immune imprinting, the humoral immune repertoire is not effectively diversified by infection of the new Omicron variants, while the immune pressure on the new variant RBD becomes more and more concentrated on these several sites. Therefore, the escaping mutation occurs on those limited number of sites. The newly emerged escaping mutations furtherly narrow down the effective antibody repertoire, which will in turn affects how the mutation occurs under concentrated immune pressure. The interaction between convergent evolution of escaping variants and less diversified antibody repertoire would ultimately lead to a highly escapable variants, posing a great challenge to current vaccines and antibody drugs. It could even be worse that infection with the predicted final convergent evolution variants may lead to increased disease severity due to the limited number of neutralizing antibodies elicited immediately after infection. Therefore, the disease severity caused by new variants needs to be closely monitored and measured in the future.

Our prediction demonstrates a remarkable consistency compared to real observations. Some variants close to the predicted and constructed variants have emerged while we performing the experiments, validating our prediction model. For example, BQ.1.1 (BA.5+R346T+K444T+N460K) is quite similar to BA.5-S3 (BA.5+R346T+N417T+K444N+N460K), given that K444N/T and K417N/T exhibited similar evasion capabilities (Fig. 4c). Together, our results suggest herd immunity established by natural infection could hardly stop RBD evolution and end the pandemic, and vaccine boosters using BA.5 may not provide sufficiently broad protection against emerging subvariants

harboring convergent mutations. Therefore, rationally designed broad-spectrum SARS-CoV-2 vaccines and NAb drugs should be in high priority and our construction of convergent mutants could serve to examine their effectiveness in advance.

Acknowledgements

We thank J. Bloom for his gift of the yeast SARS-CoV-2 RBD libraries. We thank all volunteers for providing the blood samples. This project is financially supported by the Ministry of Science and Technology of China and Changping laboratory under the project number (CPL-1233).

Author contributions

Y.C. designed the study. X.S.X supervised the study. Y.C, F.J., A.Y, Q.G. and X.S.X. wrote the manuscript with inputs from all authors. A.Y., W.S., R.A., Yao.W., and X.N. performed B cell sorting, single-cell VDJ sequencing, and antibody sequence analyses. J.W. (BIOPIC), H.S. and F.J. performed and analyzed the DMS data. Y.Y. and Youchun.W. constructed the pseudotyped virus. N.Z., P.W., L.Y., T.X. and F.S. performed the pseudotyped virus neutralization assays. W.S. and Y.C. analyzed the neutralization data. X.H., Y.X., and R.J. recruited the SARS-CoV-2 vaccinees and convalescents. J.W. (Changping Laboratory), L.Y. and F.S. performed the antibody expression.

Conflicts of interest

X.S.X and Y.C. are co-founders of Singlomics Biopharmaceuticals and listed as inventors on patents related to DXP-604, SA55, and SA58. The remaining authors declare no competing interests.

Main Figures

Fig. 1 | Convergent evolution of Omicron RBD with growth advantage over BA.5.

a, Whole-genome maximum likelihood phylogenetic analysis of Omicron subvariants. Variants with a growth advantage over the original BA.5 are colored. Relative growth advantage values

are calculated using CoV-Spectrum website. **b**, Key RBD mutations in emerging SARS-CoV-2 BA.5 and BA.2.75 subvariants exhibit convergent pattern.

Fig. 2 | Emerging Omicron subvariants further evade neutralizing antibodies.

a, IC50 of therapeutic NAbs against VSV-based pseudoviruses with spike glycoproteins of emerging SARS-CoV-2 BA.2/BA.5/BA.2.75 subvariants. green, IC50 ≤ 100ng/mL; white, 100ng/mL < IC50 < 1,000ng/mL; red, IC50 ≥ 1,000ng/mL; *, IC50 ≥ 10,000ng/mL. **b**, Relative hACE2-binding affinity measured by IC50 of hACE2 against pseudoviruses of variants. Error bars indicate mean±s.d. P-values were calculated using two-tailed Wilcoxon's rank-sum test. *, $p < 0.05$; **, $p < 0.01$; ***, $p < 0.001$. No label on variants with $p > 0.05$. Variants with significantly higher affinity are colored blue, while those with lower affinity are colored red. **c-f**, Pseudovirus-neutralizing titers against SARS-CoV-2 D614G and Omicron subvariants of plasma from vaccinated individuals or convalescents of breakthrough infection. **c**, Individuals who had received 3 doses of CoronaVac (n = 40). **d**, Convalescents who had been infected with BA.1 after receiving 3 doses of CoronaVac (n = 50). **e**, Convalescents who had been infected with BA.2 after receiving 3 doses of CoronaVac (n = 39). **f**, Convalescents who had been infected with BA.5 after receiving 3 doses of CoronaVac (n = 10). The geometric mean titers are labeled. Statistical tests are performed using two-tailed Wilcoxon signed-rank tests of paired samples. *, $p < 0.05$; **, $p < 0.01$; ***, $p < 0.001$; NS, not significant, $p > 0.05$.

Fig. 3 | Epitope characterization of mAbs from Omicron breakthrough convalescents.

a-c, FACS analysis of pooled memory B cells (IgM^-/ $CD27^+$) from Omicron convalescents. **a**, BA.5 breakthrough infection; **b**, BA.2 breakthrough infection; **c**, BA.2 convalescents without vaccination. **d**, The heavy chain variable domain SHM rate of BCRs from BA.2 breakthrough infection convalescents that bind BA.2 RBD but not WT RBD, and that are cross-reactive to WT/BA.2-RBD, and BCRs from BA.5 breakthrough infection convalescents that bind BA.5 RBD but not WT RBD, and that are cross-reactive to WT/BA.5 RBD. Binding specificity is determined by ELISA. Statistical tests are determined using two-tailed Wilcoxon signed-rank tests. Boxes show 25th percentile, median and 75th percentile, and violin plots show kernel density estimation curves of the distribution. **e**, t-SNE and clustering of SARS-CoV-2 wildtype

RBD-binding antibodies based on DMS profiles of 3051 antibodies. **f**, Epitope distribution of 680 antibodies from wildtype convalescents, 652 antibodies from post-vaccination BA.1 infection convalescents, 600 from BA.2 breakthrough infection convalescents, and 238 from BA.5 breakthrough infection convalescents. **g**, Neutralizing activity against SARS-CoV-2 D614G (n=3046), BA.2.75 (n=3045), and BA.4/5 (n=3044), respectively; and **h**, ACE2 competition level determined by competition ELISA (n=1316), were projected onto the t-SNE.

Fig. 4 | Immune imprinting promotes convergent evolution of escape mutations.

a-b, Normalized average escape scores weighted by IC50 against **a**, BA.2/BA.5 pseudovirus using DMS profiles of mAbs from corresponding convalescents. **b**, BA.2.75/BA.5 pseudovirus using DMS profiles of all mAbs except those from SARS convalescents. **c**, IC50 of representative potent BA.2-neutralizing antibodies in epitope group A, B, D1, D2, E1, E2.1, E2.2, and E3, against multiple emerging and constructed Omicron subvariants with escape mutations, in addition to IC50 of hACE2 against these variants. Error bars indicate mean±s.d. P-values were calculated using two-tailed Wilcoxon's rank-sum test. *, $p < 0.05$; **, $p < 0.01$; ***, $p < 0.001$. No label on variants with $p > 0.05$. Variants with significantly higher affinity are colored blue, while those with lower affinity are colored red. **d**, IC50 against featured Omicron subvariants of RBD-targeting mAbs from BA.1 (N=108), BA.2 (N=92), and BA.5 (N=17) breakthrough convalescents, which bind the RBD of the elicited strain but not WT. Binding specificity is determined by ELISA. The geometric mean IC50 are labeled, and error bars indicate geometric standard deviation. P-values are calculated using two-tailed Wilcoxon signed-rank tests compared to the corresponding strain. *, $p < 0.05$; **, $p < 0.01$; ***, $p < 0.001$; NS, not significant, $p > 0.05$. **e**, IC50 of NTD-targeting mAbs against BA.2, BA.2.75 and BA.2 mutants with single NTD substitution.

Fig. 5 | Accumulation of convergent escape mutations leads to complete loss of neutralization.

a, Mutations of multiple designed mutants that harbors key convergent escape mutations based on BA.2.75 and BA.5. **b**, IC50 of therapeutic mAbs and cocktails against pseudoviruses of designed mutants. green, IC50 ≤ 100ng/mL; white, 100ng/mL < IC50 < 1,000ng/mL; red, IC50

≥ 1,000ng/mL; *, IC50 ≥ 10,000ng/mL. **c**, IC50 of hACE2 against the designed mutants. Error bars indicate mean±s.d. P-values were calculated using two-tailed Wilcoxon's rank-sum test. *, $p < 0.05$; **, $p < 0.01$; ***, $p < 0.001$. No label on variants with $p > 0.05$. **d-g**, Pseudovirus neutralizing titres against SARS-CoV-2 D614G, Omicron subvariants and designed mutants of plasma from vaccinated or convalescent individuals from breakthrough infection. **d**, Individuals who received 3 doses of CoronaVac (n = 40). **e**, Convalescents infected with BA.1 after receiving 3 doses of CoronaVac (n = 50). **f**, Convalescents infected with BA.2 after receiving 3 doses of CoronaVac (n = 39). **g**, Convalescents infected with BA.5 after receiving 3 doses of CoronaVac (n = 10). Key additional mutations harbored by each designed mutant are annotated above the points. The geometric mean titers are labeled. P-values are determined using two-tailed Wilcoxon signed-rank tests of paired samples. *, $p < 0.05$; **, $p < 0.01$; ***, $p < 0.001$; NS, not significant, $p > 0.05$. Statistical test are determined using two-tailed Wilcoxon signed-rank tests.

Extended Data Figures

Extended Data Fig. 1 | Mutations on the spike glycoprotein of recently emerging Omicron subvariants.

Red grids indicate the corresponding PANGO lineage carries corresponding mutation.

Extended Data Fig. 2 | Distribution of antibody sources and neutralizing activities on the DMS landscape.

a, Sources of the 3051 mAbs involved in this study projected on the t-SNE of DMS profiles. **b**, IC50 against SARS-CoV-1 (N=1870 determined), Omicron BA.1 (N=2933), BA.2 (N=3044) of these mAbs projected on the embedding.

Extended Data Fig. 3 | Escape hotspots and neutralization of mAbs in epitope group A, B and C

a-c, Average escape scores of epitope group A (**a**), B (**b**), C (**c**) and on each RBD residue are projected onto the structure of SARS-CoV-2 RBD (PDB: 6M0J). And average escape maps at

escape hotspots of antibodies, grouped by their sources, in epitope group A (**a**), B (**b**) and C (**c**), and corresponding sequence alignment of SARS-CoV-2 WT and Omicron RBDs. Height of each amino acid in the escape maps represents its mutation escape score. Mutated sites in Omicron variants are marked in bold. **d**, Pseudovirus-neutralizing IC50 of antibodies in group A, B, and C, from wildtype convalescents or vaccinees (WT-elicited, n=133, 50, 106 for A-C, respectively), BA.1 convalescents (BA.1-elicited, n=51, 49, 24), BA.2 convalescents (BA.2-elicited, n=34, 36, 56) and BA.5 convalescents (BA.5-elicited, n=16, 6, 14). The geometric mean IC50 are labeled, and error bars indicate geometric standard deviation. P-values are calculated using two-tailed Wilcoxon signed-rank tests. *, $p < 0.05$; **, $p < 0.01$; ***, $p < 0.001$; NS, not significant, $p > 0.05$.

Extended Data Fig. 4 | Escape hotspots and neutralization of mAbs in epitope group D and E1

a-d, Similar to Extended Data Fig. 3, but for epitope group D1, D2, and E1. **d**, For WT-elicited mAbs, n=49, 37, 19 for D1, D2 and E1, respectively; For BA.1-elicited, n=59, 21, 14; For BA.2-elicited, n=56, 15, 9; For BA.5-elicited, n=14, 17, 9.

Extended Data Fig. 5 | Escape hotspots and neutralization of mAbs in epitope group E2 and E3

a-d, Similar to Extended Data Fig. 3 and 4, but for epitope group E2.1, E2.2, and E3. **d**, For WT-elicited mAbs, n=35, 69, 63 for E2.1, E2.2 and E3, respectively; For BA.1-elicited, n=81, 159, 89; For BA.2-elicited, n=53, 132, 106; For BA.5-elicited, n=11, 85, 36.

Extended Data Fig. 6 | Predicted escape hotspots of SARS-CoV-2 variants

a, Normalized average escape scores weighted by IC50 against D614G using DMS profiles of mAbs from ancestral strain infection or vaccination with a logo plot showing specific mutations on important residues. **b**, Normalized average escape scores of mAbs from BA.1 breakthrough infection, weighted by IC50 against BA.1. **c**, Normalized average escape scores of mAbs from ancestral strain infection or vaccination and BA.1 breakthrough infection, weighted by IC50 against BA.2. Including BA.2-elicited mAbs does not cause substantial change. **d**,

WT/BA.1/BA.2-elicited mAbs with IC50 against BA.2.75 and BA.5, similar to Fig. 4b.

Extended Data Fig. 7 | IC50 heatmap of representative mAbs against constructed Omicron variants.

a, Color shades indicate IC50 of antibodies (columns) against constructed Omicron BA.2 or BA.5 subvariants (rows) carrying mutations on the epitope of each group. The order of mAbs is the same as Figure 4c. **b**, IC50 of NTD-targeting antibodies against SARS-CoV-2 variants, which is related to Fig. 4e.

Method

Isolation of peripheral blood mononuclear cells and plasma

Samples from vaccinees and individuals who had recovered from BA.1, BA.2, or BA.5 infection were obtained under study protocols approved by Beijing Ditan Hospital, Capital Medical University (Ethics committee archiving No. LL-2021-024-02) and the Tianjin Municipal Health Commission, and the Ethics Committee of Tianjin First Central Hospital (Ethics committee archiving No. 2022N045KY). All donors provided written informed consent for the collection of information, the use of blood and blood components, and publication of data generated from this study. Whole blood sample were diluted 1:1 with PBS+2% FBS (Gibco) and subjected to Ficoll (Cytiva) gradient centrifugation. Plasma was collected from upper layer. Cells were collected at the interface and further prepared by centrifugation, red blood cells lysis (Invitrogen eBioscience) and washing steps.

BCR sequencing, analysis, and antibody production.

CD19+ B cells were isolated from PBMCs with EasySep Human CD19 Positive Selection Kit II (STEMCELL, 17854). Every 10^6 B cells in 100 µl solution were stained with 3 µl FITC anti-human CD20 antibody (BioLegend, 302304, clone: 2H7), 3.5 µl Brilliant Violet 421 anti-human CD27 antibody (BioLegend, 302824, clone: O323), 2 µl PE/Cyanine7 anti-human IgM antibody (BioLegend, 314532, clone: MHM-88), 2 µl PE/Cyanine7 anti-human IgD antibody (BioLegend, 348210, clone: IA6-2), 0.13 µg biotinylated SARS-CoV-2 BA.2 RBD protein

(customized from Sino Biological) or 0.13 μg biotinylated SARS-CoV-2 BA.5 RBD protein (customized from Sino Biological) conjugated with PE-streptavidin (BioLegend, 405204) or APC-streptavidin (BioLegend, 405207), 0.13 μg SARS-CoV-2 WT biotinylated RBD protein (Sino Biological, 40592-V27H-B) conjugated with Brilliant Violet 605 Streptavidin (BioLegend, 405229). Cells are also labeled with biotinylated RBD conjugated to DNA-oligo-streptavidin. Cells were washed twice after 30 minutes incubation on ice. 7-AAD (Invitrogen, 00-6993-50) were used to label dead cells. 7-AAD−CD20+CD27+IgM−IgD− SARS-CoV-2 BA.2 RBD+ or BA.5+ cells were sorted with a MoFlo Astrios EQ Cell Sorter. FACS data were analysed using FlowJo v10.8 (BD Biosciences).

Sorted B cells were resuspended in appropriate volume and then processed with Chromium Next GEM Single Cell V(D)J Reagent Kits v1.1 following the manufacturer's user guide (10x Genomics, CG000208). Gel beads-in-emulsion (GEMs) were obtained with 10X Chromium controller. GEMs were subjected to reverse transcription and purification. Reverse transcription products were subject to preamplification and purification with SPRIselect Reagent Kit (Beckman Coulter, B23318). BCR sequences (paired V(D)J) were enriched with 10X BCR primers. After library preparation, libraries were sequenced with illumina sequencing platform.

10X Genomics V(D)J sequencing data were assembled as BCR contigs and aligned using Cell Ranger (v6.1.1) pipeline according to the GRCh38 BCR reference. Only the productive contigs and the B cells with one heavy chain and one light chain were kept for quality control. The germline V(D)J gene identification and annotation were performed by IgBlast (v1.17.1)[47]. Somatic hypermutation sites in the antibody variable domain were detected using Change-O toolkit (v1.2.0)[48].

Antibody heavy and light chain genes were optimized for human cell expression and synthesized by GenScript. VH and VL were inserted separately into plasmids (pCMV3-CH, pCMV3-CL or pCMV3-CK) through infusion (Vazyme, C112). Plasmids encoding heavy chain and light chain of antibodies were co-transfected by polyethylenimine-transfection to Expi293F™ cell (ThermoFisher, A14527). Cells were cultured at 36.5℃, 5% CO2, 175 rpm

for 6-10 days. Supernatants containing mAbs were collected, and the supernatants were further purified with protein A magnetic beads (Genscript, L00695).

High-throughput mutation escape profiling

High-throughput mutation escape profiling platform has been described previously[1,2]. Briefly, deep mutation scanning libraries were constructed by mutagenesis PCR based on Wuhan-Hu-1 RBD sequence (GenBank: MN908947, residues N331-T531). BA.1 and BA.2 RBD mutant libraries were created in a similar way with the addition of respective substitutions, respectively. A unique 26-neuclotide (N26) barcode was appended to each RBD variant in mutant libraries by PCR and the correspondence between N26 barcode and mutations in RBD variants was acquired by PacBio sequencing. RBD mutant libraries were first transformed in EBY100 strain of *Saccharomyces cerevisiae* and then enriched for properly folded ACE2 binders, which were used for subsequent mutation escape profiling. The above ACE2 binders were grown in SG-CAA media (2% w/v d-galactose, 0.1% w/v dextrose (d-glucose), 0.67% w/v yeast nitrogen base, 0.5% w/v casamino acids (−ade, −ura, −trp), 100 mM phosphate buffer, pH 6.0) at room temperature for 16-18h with agitation. Then these yeast cells were washed twice and proceeded to three rounds of magnetic beads-based selection. Obtained yeast cells after sequential sorting were recovered overnight in SD-CAA media (2% w/v dextrose (d-glucose), 0.67% w/v yeast nitrogen base, 0.5% w/v casamino acids (−ade, −ura, −trp), 70 mM citrate buffer, pH 4.5). Pre- and post-sort yeast populations were submitted to plasmid extraction by 96 Well Plate Yeast Plasmid Preps Kit (Coolaber, PE053). N26 barcode sequences were amplified with the extracted plasmid templates and PCR products were purified and submitted to Illumina Nextseq 550 sequencing.

Antibody clustering and embedding based on DMS profiles

Data analysis of DMS were performed as described in previous reports [1,2]. In brief, the detected barcode sequences of both the antibody-screened and reference library were aligned to the barcode-variant lookup table generated using dms_variants (v0.8.9). The escape scores of each variant X in the library were defined as $F\times(n_{X,ab} / N_{ab}) / (n_{X,ref} / N_{ref})$, where F is a scale factor to normalize the scores to 0-1 range, while n and N are the number of detected barcodes for

variant X and total barcodes in post-selected (ab) or reference (ref) samples, respectively. The escape scores of each mutation were calculated by fitting an epistasis model as described previously [41,49].

Epitope groups of new antibodies that did not included in our previous report are determined by k-nearest neighbors (KNN)-based classification. In brief, site escape scores of each antibody are first normalized and considered as a distribution across RBD residues, and only residues whose standard derivation is among the highest 50% of all residues are retained for further analysis. Then the dissimilarity or distance of two antibodies is defined by the Jessen-Shannon divergence of the normalized escape scores. Pair-wise dissimilarities of all antibodies in the dataset are calculated using scipy package (scipy.spatial.distance.jensenshannon, v1.7.0). For each antibody, 15 nearest neighbors whose epitope group have been determined by unsupervised clustering in our previous paper are identified and simply voted to determine the group of the selected antibody. To project the dataset onto a 2D space for visualization, we performed MDS to represent each antibody in a 32-dimensional space, and then t-SNE to get the 2D representation, using sklearn.manifold.MDS and sklearn.manifold.TSNE (v0.24.2).

Calculation of the estimated preference of RBD mutations

Four different weights are included in the calculation, including the weight for ACE2-binding affinity, RBD expression, codon constraint, and neutralizing activity. Impact on ACE2-binding affinity and RBD expression of each mutation based on WT, BA.1 and BA.2 are obtained from public DMS results. And for BA.5 (BA.2+L452R+F486V+R493Q) and BA.2.75 (BA.2+D339H+G446S+N460K+R493Q), BA.2 results are used except for these mutated residues, whose scores for each mutant are subtracted by the score for the mutation in BA.5 or BA.2.75. As the reported values are log fold changes, the weight is simply defined by the exponential of reported values, i.e. $\exp[S_{\mathrm{bind}}]$ or $\exp[S_{\mathrm{expr}}]$ respectively. For codon constraint, the weight is 1.0 for mutants that could be accessed by one nucleotide mutation, and 0.0 for others. We used the following RBD nucleotide sequences for determination of accessible mutants, WT/D614G (Wuhan-Hu-1 reference genome), BA.1 (EPI_ISL_10000028), BA.2 (EPI_ISL_10000005), BA.4/5 (EPI_ISL_11207535), BA.2.75 (EPI_ISL_13302209).

For neutralizing activity, the weight is -$\log_{10}$(IC50). The IC50 values (μg/mL) which are smaller than 0.0005 or larger than 1.0 are considered as 0.0005 or 1.0, respectively. The raw escape scores for each antibody are first normalized by the max score among all mutants, and the final weighted score for each antibody and each mutation is the production of the normalized scores and four corresponding weights. The final mutation-specific weighted score is the summation of scores of all antibodies in the designated antibody set, and then normalized again to make it a value between 0 and 1. Logo plots for visualization of escape maps were generated by Python package logomaker (v0.8).

Pseudotyped-virus assay

The Spike gene (GenBank: MN908947) was mammalian condon-opimized and inserted into pcDNA3.1 vector. Site directed mutagenesis PCR was performed as described previously[50]. Sequence of mutants are shown in Fig. S1. Pseudotyped viruses were generated by transfection 293T cells (ATCC, CRL-3216) with pcDNA3.1-Spike with Lipofectamine 3000 (Invitrogen). The cells were subsequently infected with G*ΔG-VSV (Kerafast) that packages expression cassettes for firefly luciferase instead of VSV-G in the VSV genome. The cell supernatants were discarded after 6-8h harvest and replaced with complete culture media. The cell was cultured one day and then the cell supernatant containing pseudotyped virus was harvested, filtered (0.45-μm pore size, Millipore), aliquoted, and stored at -80 °C. Viruses of multiple variants were diluted to the same number of copies before use.

mAbs or plasma were serially diluted and incubated with the pseudotyped virus in 96-well plates for 1 h at 37°C. Trypsin-treated Huh-7 cells (Japanese Collection of Research Bioresources, Cat0403) were added to the plate. The cells were cultured for 20-28 h in 5% CO_2, 37°C incubator. The supernatants were removed and leave 100 μL in each well and 100 μL luciferase substrate (Perkinelmer, 6066769) were added and incubate in dark for 2 min. The cell lysate was removed to white solid plates and the chemiluminescence signals were collected by PerkinElmer Ensight. Each experiment was repeated for at least twice.

Dulbecco's modified Eagle medium (DMEM, high glucose; HyClone) with 100 U/mL of

penicillin–streptomycin solution (Gibco), 20 mM N-2-hydroxyethylpiperazine-N-2-ethane sulfonic acid (HEPES, Gibco) and 10% fetal bovine serum (FBS, Gibco) were used in cell culture. Trypsin-EDTA (0.25%, Gibco) was used to detach cells before seeding to the plate.

References

1 Cao, Y. *et al.* Omicron escapes the majority of existing SARS-CoV-2 neutralizing antibodies. *Nature* **602**, 657-663, doi:10.1038/s41586-021-04385-3 (2022).

2 Cao, Y. *et al.* BA.2.12.1, BA.4 and BA.5 escape antibodies elicited by Omicron infection. *Nature* **608**, 593-602, doi:10.1038/s41586-022-04980-y (2022).

3 Iketani, S. *et al.* Antibody evasion properties of SARS-CoV-2 Omicron sublineages. *Nature* **604**, 553-556, doi:10.1038/s41586-022-04594-4 (2022).

4 Wang, Q. *et al.* Antibody evasion by SARS-CoV-2 Omicron subvariants BA.2.12.1, BA.4 and BA.5. *Nature* **608**, 603-608, doi:10.1038/s41586-022-05053-w (2022).

5 Tuekprakhon, A. *et al.* Antibody escape of SARS-CoV-2 Omicron BA.4 and BA.5 from vaccine and BA.1 serum. *Cell* **185**, 2422-2433 e2413, doi:10.1016/j.cell.2022.06.005 (2022).

6 Uraki, R. *et al.* Characterization and antiviral susceptibility of SARS-CoV-2 Omicron/BA.2. *Nature*, doi:10.1038/s41586-022-04856-1 (2022).

7 Liu, L. *et al.* Striking antibody evasion manifested by the Omicron variant of SARS-CoV-2. *Nature* **602**, 676-681, doi:10.1038/s41586-021-04388-0 (2022).

8 Cele, S. *et al.* Omicron extensively but incompletely escapes Pfizer BNT162b2 neutralization. *Nature* **602**, 654-656, doi:10.1038/s41586-021-04387-1 (2022).

9 Cameroni, E. *et al.* Broadly neutralizing antibodies overcome SARS-CoV-2 Omicron antigenic shift. *Nature* **602**, 664-670, doi:10.1038/s41586-021-04386-2 (2022).

10 Yamasoba, D. *et al.* Virological characteristics of the SARS-CoV-2 Omicron BA.2 spike. *Cell* **185**, 2103-2115 e2119, doi:10.1016/j.cell.2022.04.035 (2022).

11 Nutalai, R. *et al.* Potent cross-reactive antibodies following Omicron breakthrough in vaccinees. *Cell* **185**, 2116-2131 e2118, doi:10.1016/j.cell.2022.05.014 (2022).

12 Dejnirattisai, W. *et al.* SARS-CoV-2 Omicron-B.1.1.529 leads to widespread escape from neutralizing antibody responses. *Cell* **185**, 467-484 e415, doi:10.1016/j.cell.2021.12.046 (2022).

13 Cui, Z. *et al.* Structural and functional characterizations of infectivity and immune evasion of SARS-

CoV-2 Omicron. *Cell* **185**, 860-871 e813, doi:10.1016/j.cell.2022.01.019 (2022).

14 Wang, K. *et al.* Memory B cell repertoire from triple vaccinees against diverse SARS-CoV-2 variants. *Nature* **603**, 919-925, doi:10.1038/s41586-022-04466-x (2022).

15 Kimura, I. *et al.* Virological characteristics of the SARS-CoV-2 Omicron BA.2 subvariants including BA.4 and BA.5. *Cell*, doi:10.1016/j.cell.2022.09.018.

16 Shu, Y. & McCauley, J. GISAID: Global initiative on sharing all influenza data – from vision to reality. *Eurosurveillance* **22**, 30494, doi:doi:https://doi.org/10.2807/1560-7917.ES.2017.22.13.30494 (2017).

17 Rambaut, A. *et al.* A dynamic nomenclature proposal for SARS-CoV-2 lineages to assist genomic epidemiology. *Nature Microbiology* **5**, 1403-1407, doi:10.1038/s41564-020-0770-5 (2020).

18 Wang, Q. *et al.* Antigenic characterization of the SARS-CoV-2 Omicron subvariant BA.2.75. *Cell Host & Microbe*, doi:https://doi.org/10.1016/j.chom.2022.09.002 (2022).

19 Sheward, D. J. *et al.* Evasion of neutralising antibodies by omicron sublineage BA.2.75. *Lancet Infect Dis*, doi:10.1016/S1473-3099(22)00524-2 (2022).

20 Cao, Y. *et al.* Characterizations of enhanced infectivity and antibody evasion of Omicron BA.2.75. *bioRxiv*, 2022.2007.2018.500332, doi:10.1101/2022.07.18.500332 (2022).

21 Jian, F. *et al.* Further humoral immunity evasion of emerging SARS-CoV-2 BA.4 and BA.5 subvariants. *bioRxiv*, 2022.2008.2009.503384, doi:10.1101/2022.08.09.503384 (2022).

22 Saito, A. *et al.* Virological characteristics of the SARS-CoV-2 Omicron BA.2.75. *bioRxiv*, 2022.2008.2007.503115, doi:10.1101/2022.08.07.503115 (2022).

23 Chen, C. *et al.* CoV-Spectrum: Analysis of Globally Shared SARS-CoV-2 Data to Identify and Characterize New Variants. *Bioinformatics* **38**, 1735-1737, doi:10.1093/bioinformatics/btab856 (2021).

24 Greaney, A. J. *et al.* Comprehensive mapping of mutations in the SARS-CoV-2 receptor-binding domain that affect recognition by polyclonal human plasma antibodies. *Cell Host Microbe* **29**, 463-476 e466, doi:10.1016/j.chom.2021.02.003 (2021).

25 Greaney, A. J. *et al.* Complete Mapping of Mutations to the SARS-CoV-2 Spike Receptor-Binding Domain that Escape Antibody Recognition. *Cell Host Microbe* **29**, 44-57 e49, doi:10.1016/j.chom.2020.11.007 (2021).

26 Greaney, A. J. *et al.* Mapping mutations to the SARS-CoV-2 RBD that escape binding by different classes of antibodies. *Nature Communications* **12**, 4196, doi:10.1038/s41467-021-24435-8 (2021).

27 Copin, R. *et al.* The monoclonal antibody combination REGEN-COV protects against SARS-CoV-2

mutational escape in preclinical and human studies. *Cell* **184**, 3949-3961 e3911, doi:10.1016/j.cell.2021.06.002 (2021).

28 Zost, S. J. *et al.* Potently neutralizing and protective human antibodies against SARS-CoV-2. *Nature* **584**, 443-449, doi:10.1038/s41586-020-2548-6 (2020).

29 Self, W. H. *et al.* Efficacy and safety of two neutralising monoclonal antibody therapies, sotrovimab and BRII-196 plus BRII-198, for adults hospitalised with COVID-19 (TICO): a randomised controlled trial. *Lancet Infectious Diseases* **22**, 622-635, doi:10.1016/S1473-3099(21)00751-9 (2022).

30 Pinto, D. *et al.* Cross-neutralization of SARS-CoV-2 by a human monoclonal SARS-CoV antibody. *Nature* **583**, 290-295, doi:10.1038/s41586-020-2349-y (2020).

31 Westendorf, K. *et al.* LY-CoV1404 (bebtelovimab) potently neutralizes SARS-CoV-2 variants. *Cell Rep* **39**, 110812, doi:10.1016/j.celrep.2022.110812 (2022).

32 Cao, Y. *et al.* Rational identification of potent and broad sarbecovirus-neutralizing antibody cocktails from SARS convalescents. *bioRxiv*, 2022.2008.2003.499114, doi:10.1101/2022.08.03.499114 (2022).

33 Loo, Y. M. *et al.* The SARS-CoV-2 monoclonal antibody combination, AZD7442, is protective in nonhuman primates and has an extended half-life in humans. *Sci Transl Med* **14**, eabl8124, doi:10.1126/scitranslmed.abl8124 (2022).

34 Starr, T. N., Greaney, A. J. & Bloom, J. D. *Deep mutational scanning of the SARS-CoV-2 RBD in Omicron BA.1 and BA.2 variant backgrounds*, <https://jbloomlab.github.io/SARS-CoV-2-RBD_DMS_Omicron/RBD-heatmaps/> (2022).

35 Gao, Q. *et al.* Development of an inactivated vaccine candidate for SARS-CoV-2. *Science* **369**, 77-81, doi:10.1126/science.abc1932 (2020).

36 Quandt, J. *et al.* Omicron BA.1 breakthrough infection drives cross-variant neutralization and memory B cell formation against conserved epitopes. *Sci Immunol*, eabq2427, doi:10.1126/sciimmunol.abq2427 (2022).

37 Khan, K. *et al.* Omicron BA.4/BA.5 escape neutralizing immunity elicited by BA.1 infection. *Nature Communications* **13**, 4686, doi:10.1038/s41467-022-32396-9 (2022).

38 Park, Y. J. *et al.* Imprinted antibody responses against SARS-CoV-2 Omicron sublineages. *bioRxiv*, 2022.2005.2008.491108, doi:10.1101/2022.05.08.491108 (2022).

39 Reynolds, C. J. *et al.* Immune boosting by B.1.1.529 (Omicron) depends on previous SARS-CoV-2 exposure. *Science* **377**, eabq1841, doi:10.1126/science.abq1841 (2022).

40 Greaney, A. J., Starr, T. N. & Bloom, J. D. An antibody-escape estimator for mutations to the SARS-CoV-2 receptor-binding domain. *Virus Evol* **8**, veac021, doi:10.1093/ve/veac021 (2022).

41 Starr, T. N. *et al.* Deep Mutational Scanning of SARS-CoV-2 Receptor Binding Domain Reveals Constraints on Folding and ACE2 Binding. *Cell* **182**, 1295-1310 e1220, doi:10.1016/j.cell.2020.08.012 (2020).

42 Starr, T. N. *et al.* Shifting mutational constraints in the SARS-CoV-2 receptor-binding domain during viral evolution. *Science* **377**, 420-424, doi:10.1126/science.abo7896 (2022).

43 Muik, A. *et al.* Omicron BA.2 breakthrough infection enhances cross-neutralization of BA.2.12.1 and BA.4/BA.5. *bioRxiv*, 2022.2008.2002.502461, doi:10.1101/2022.08.02.502461 (2022).

44 Wang, Z. *et al.* Analysis of memory B cells identifies conserved neutralizing epitopes on the N-terminal domain of variant SARS-Cov-2 spike proteins. *Immunity* **55**, 998-1012 e1018, doi:10.1016/j.immuni.2022.04.003 (2022).

45 Chi, X. *et al.* A neutralizing human antibody binds to the N-terminal domain of the Spike protein of SARS-CoV-2. *Science* **369**, 650-655, doi:doi:10.1126/science.abc6952 (2020).

46 Witte, L. *et al.* Epistasis lowers the genetic barrier to SARS-CoV-2 neutralizing antibody escape. *bioRxiv*, 2022.2008.2017.504313, doi:10.1101/2022.08.17.504313 (2022).

47 Ye, J., Ma, N., Madden, T. L. & Ostell, J. M. IgBLAST: an immunoglobulin variable domain sequence analysis tool. *Nucleic Acids Res* **41**, W34-40, doi:10.1093/nar/gkt382 (2013).

48 Gupta, N. T. *et al.* Change-O: a toolkit for analyzing large-scale B cell immunoglobulin repertoire sequencing data. *Bioinformatics* **31**, 3356-3358, doi:10.1093/bioinformatics/btv359 (2015).

49 Otwinowski, J., McCandlish, D. M. & Plotkin, J. B. Inferring the shape of global epistasis. *Proc Natl Acad Sci U S A* **115**, E7550-E7558, doi:10.1073/pnas.1804015115 (2018).

50 Nie, J. *et al.* Quantification of SARS-CoV-2 neutralizing antibody by a pseudotyped virus-based assay. *Nat Protoc* **15**, 3699-3715, doi:10.1038/s41596-020-0394-5 (2020).

Figure 1

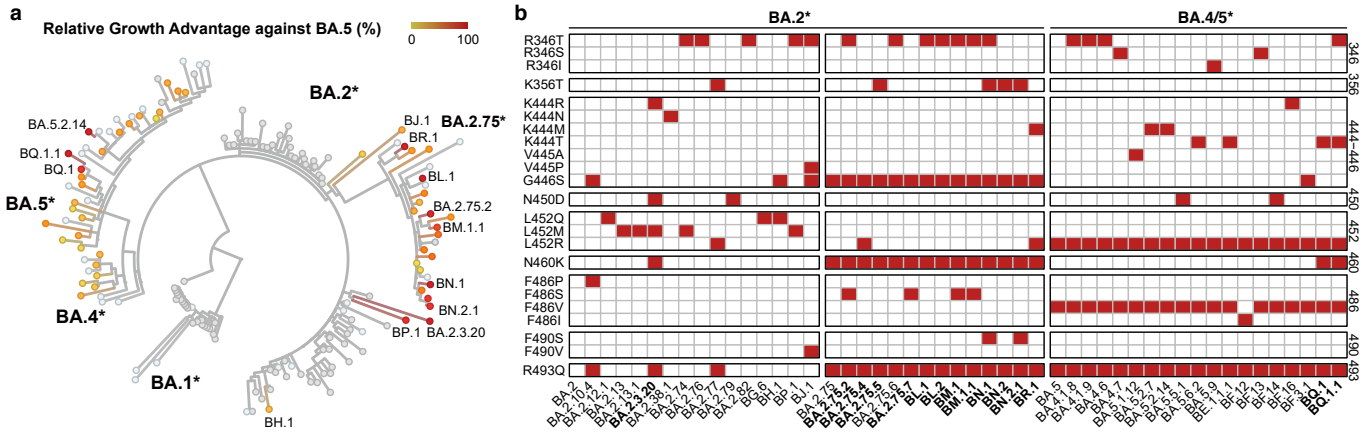

Fig. 1 | Convergent evolution of Omicron RBD with growth advantage over BA.5.
a, Whole-genome maximum likelihood phylogenetic analysis of Omicron subvariants. Variants with a growth advantage over the original BA.5 are colored. Relative growth advantage values are calculated using CoV-Spectrum website. b, Key RBD mutations in emerging SARS-CoV-2 BA.5 and BA.2.75 subvariants

Figure 2

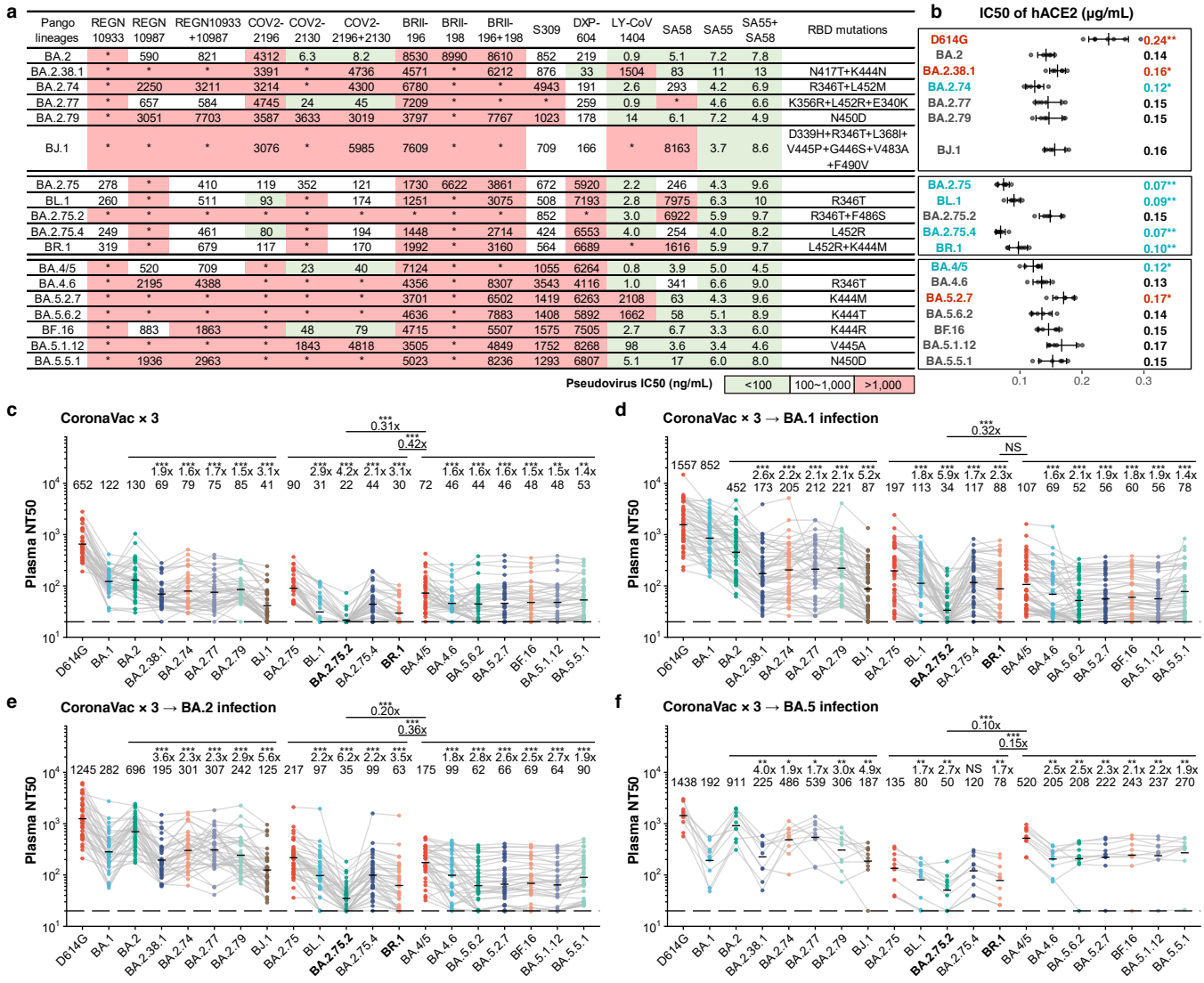

Pango lineages	REGN 10933	REGN 10987	REGN10933 +10987	COV2-2196	COV2-2130	COV2-2196+2130	BRII-196	BRII-198	BRII-196+198	S309	DXP-604	LY-CoV 1404	SA58	SA55	SA55+ SA58	RBD mutations
BA.2	*	590	821	4312	6.3	8.2	8530	8990	8610	852	219	0.9	5.1	7.2	7.8	
BA.2.38.1	*	*	*	3391	*	4736	4571	*	6212	876	33	1504	83	11	13	N417T+K444N
BA.2.74	*	2250	3211	3214	*	4300	6780	*	*	4943	191	2.6	293	4.2	6.9	R346T+L452M
BA.2.77	*	657	584	4745	24	45	7209	*	*	*	259	0.9	*	4.6	6.6	K356R+L452R+E340K
BA.2.79	*	3051	7703	3587	3633	3019	3797	*	7767	1023	178	14	6.1	7.2	4.9	N450D
BJ.1	*	*	*	3076	*	5985	7609	*	*	709	166	*	8163	3.7	8.6	D339H+R346T+L368I+ V445P+G446S+V483A +F490V
BA.2.75	278	*	410	119	352	121	1730	6622	3861	672	5920	2.2	246	4.3	9.6	
BL.1	260	*	511	93	*	174	1251	*	3075	508	7193	2.8	7975	6.3	10	R346T
BA.2.75.2	*	*	*	*	*	*	*	*	*	852	*	3.0	6922	5.9	9.7	R346T+F486S
BA.2.75.4	249	*	461	80	*	194	1448	*	2714	424	6553	4.0	254	4.0	8.2	L452R
BR.1	319	*	679	117	*	170	1992	*	3160	564	6689	*	1616	5.9	9.7	L452R+K444M
BA.4/5	*	520	709	*	23	40	7124	*	*	1055	6264	0.8	3.9	5.0	4.5	
BA.4.6	*	2195	4388	*	*	*	4356	*	8307	3543	4116	1.0	341	6.6	9.0	R346T
BA.5.2.7	*	*	*	*	*	*	3701	*	6502	1419	6263	2108	63	4.3	9.6	K444M
BA.5.6.2	*	*	*	*	*	*	4636	*	7883	1408	5892	1662	58	5.1	8.9	K444T
BF.16	*	883	1863	*	48	79	4715	*	5507	1575	7505	2.7	6.7	3.3	6.0	K444R
BA.5.1.12	*	*	*	*	1843	4818	3505	*	4849	1752	8268	98	3.6	3.4	4.6	V445A
BA.5.5.1	*	1936	2963	*	*	*	5023	*	8236	1293	6807	5.1	17	6.0	8.0	N450D

Fig. 2 | Emerging Omicron subvariants further evade neutralizing antibodies.
a, IC50 of therapeutic NAbs against VSV-based pseudoviruses with spike glycoproteins of emerging SARS-CoV-2 BA.2/BA.5/BA.2.75 subvariants. green, IC50 ≤ 100ng/mL; white, 100ng/mL < IC50 < 1,000ng/mL; red, IC50 ≥ 1,000ng/mL; *, IC50 ≥ 10,000ng/mL. b, Relative hACE2-binding affinity measured by IC50 of hACE2 against pseudoviruses of variants. Error bars indicate mean±s.d. P-values were calculated using two-tailed Wilcoxon's rank-sum test. *, $p < 0.05$; **, $p < 0.01$; ***, $p < 0.001$. No label on variants with $p > 0.05$. Variants with significantly higher affinity are colored blue, while those with lower affinity are colored red. c-f, Pseudovirus-neutralizing titers against SARS-CoV-2 D614G and Omicron subvariants of plasma from vaccinated individuals or convalescents of breakthrough infection. c, Individuals who had received 3 doses of CoronaVac (n = 40). d, Convalescents who had been infected with BA.1 after receiving 3 doses of CoronaVac (n = 50). e, Convalescents who had been infected with BA.2 after receiving 3 doses of CoronaVac (n = 39). f, Convalescents who had been infected with BA.5 after receiving 3 doses of CoronaVac (n = 10). The geometric mean titers are labeled. Statistical tests are performed using two-tailed Wilcoxon signed-rank tests of paired samples. *, $p < 0.05$; **, $p < 0.01$; ***, $p < 0.001$; NS, not significant, $p > 0.05$.

Figure 3

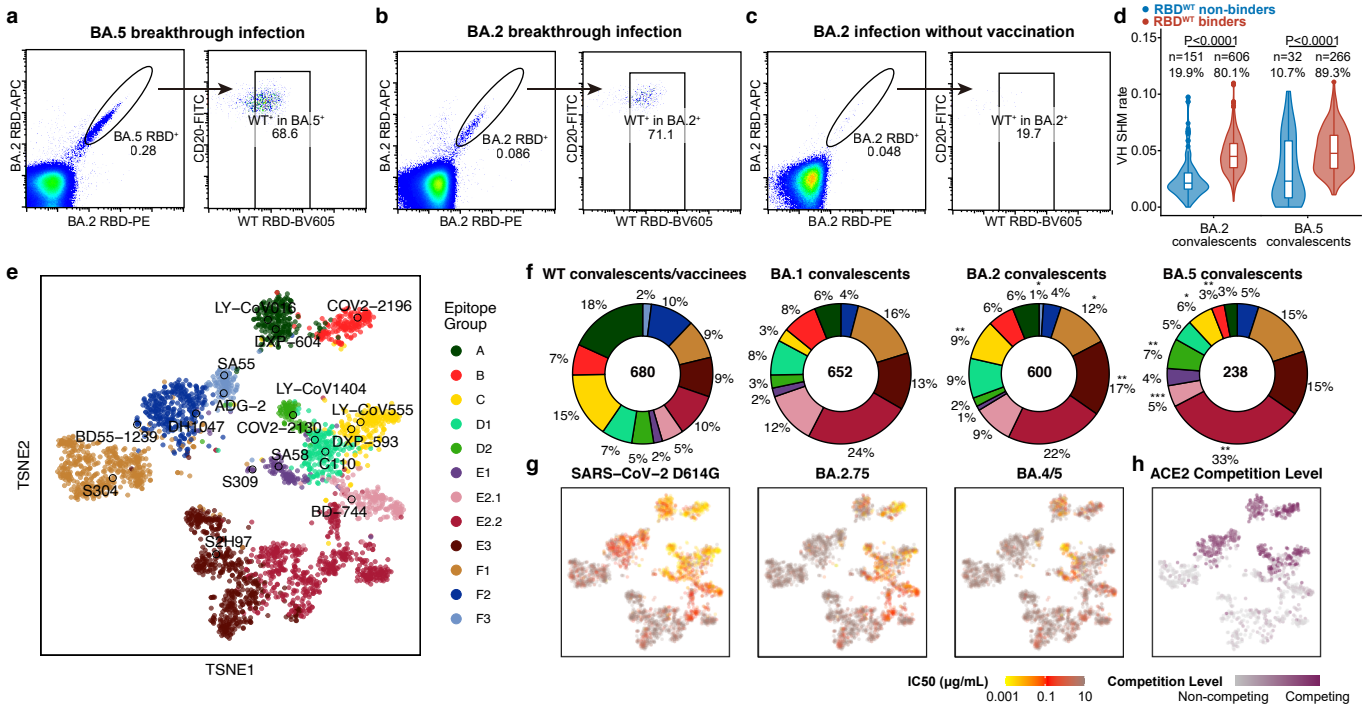

Fig. 3 | Epitope characterization of mAbs from Omicron breakthrough convalescents.
a-c, FACS analysis of pooled memory B cells (IgM-/ CD27+) from Omicron convalescents. a, BA.5 breakthrough infection; b, BA.2 breakthrough infection; c, BA.2 convalescents without vaccination. d, The heavy chain variable domain SHM rate of BCRs from BA.2 breakthrough infection convalescents that bind BA.2 RBD but not WT RBD, and that are cross-reactive to WT/BA.2-RBD, and BCRs from BA.5 breakthrough infection convalescents that bind BA.5 RBD but not WT RBD, and that are cross-reactive to WT/BA.5 RBD. Binding specificity is determined by ELISA. Statistical test are determined using two-tailed Wilcoxon signed-rank tests. Boxes show 25th percentile, median and 75th percentile, and violin plots show kernel density estimation curves of the distribution. e, t-SNE and clustering of SARS-CoV-2 wildtype RBD-binding antibodies based on DMS profiles of 3051 antibodies. f, Epitope distribution of 680 antibodies from wildtype convalescents, 652 antibodies from post-vaccination BA.1 infection convalescents, 600 from BA.2 breakthrough infection convalescents, and 238 from BA.5 breakthrough infection convalescents. g, Neutralizing activity against SARS-CoV-2 D614G (n=3046), BA.2.75 (n=3045), and BA.4/5 (n=3044), respectively; and h, ACE2 competition level determined by competition ELISA (n=1316), were projected onto the t-SNE.

Figure 4

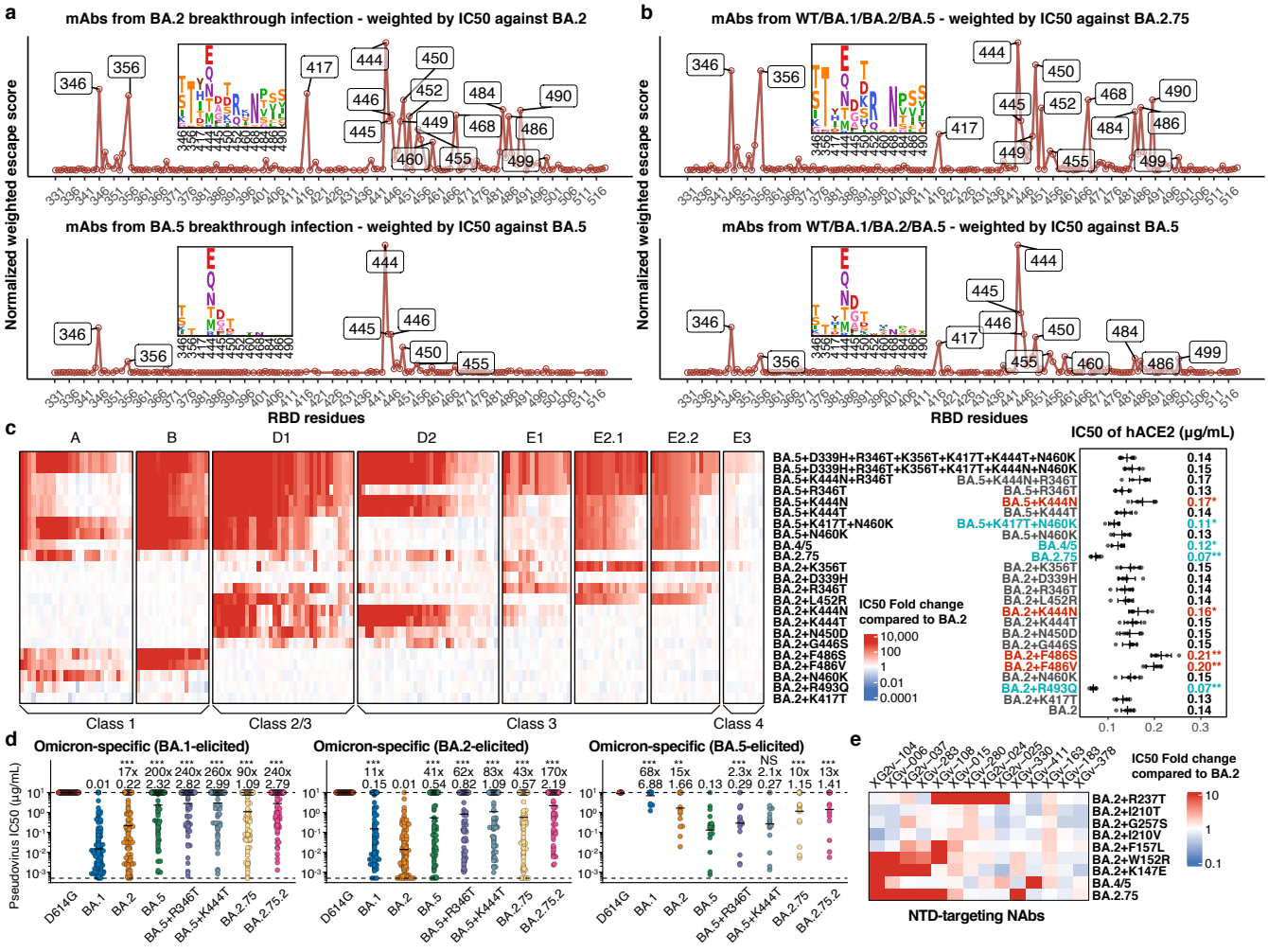

Fig. 4 | Immune imprinting promotes convergent evolution of escape mutations.
a-b, Normalized average escape scores weighted by IC50 against a, BA.2/BA.5 pseudovirus using DMS profiles of mAbs from corresponding convalescents. b, BA.2.75/BA.5 pseudovirus using DMS profiles of all mAbs except those from SARS convalescents. c, IC50 of representative potent BA.2-neutralizing antibodies in epitope group A, B, D1, D2, E1, E2.1, E2.2, and E3, against multiple emerging and constructed Omicron subvariants with escape mutations, in addition to IC50 of hACE2 against these variants. Error bars indicate mean±s.d. P-values were calculated using two-tailed Wilcoxon's rank-sum test. *, $p < 0.05$; **, $p < 0.01$; ***, $p < 0.001$. No label on variants with $p > 0.05$. Variants with significantly higher affinity are colored blue, while those with lower affinity are colored red. d, IC50 against featured Omicron subvariants of RBD-targeting mAbs from BA.1 (N=108), BA.2 (N=92), and BA.5 (N=17) breakthrough convalescents, which bind the RBD of the elicited strain but not WT. Binding specificity is determined by ELISA. The geometric mean IC50 are labeled, and error bars indicate geometric standard deviation. P-values are calculated using two-tailed Wilcoxon signed-rank tests compared to the corresponding strain. *, $p < 0.05$; **, $p < 0.01$; ***, $p < 0.001$; NS, not significant, $p > 0.05$. e, IC50 of NTD-targeting mAbs against BA.2, BA.2.75 and BA.2 mutants with single NTD substitution.

Figure 5

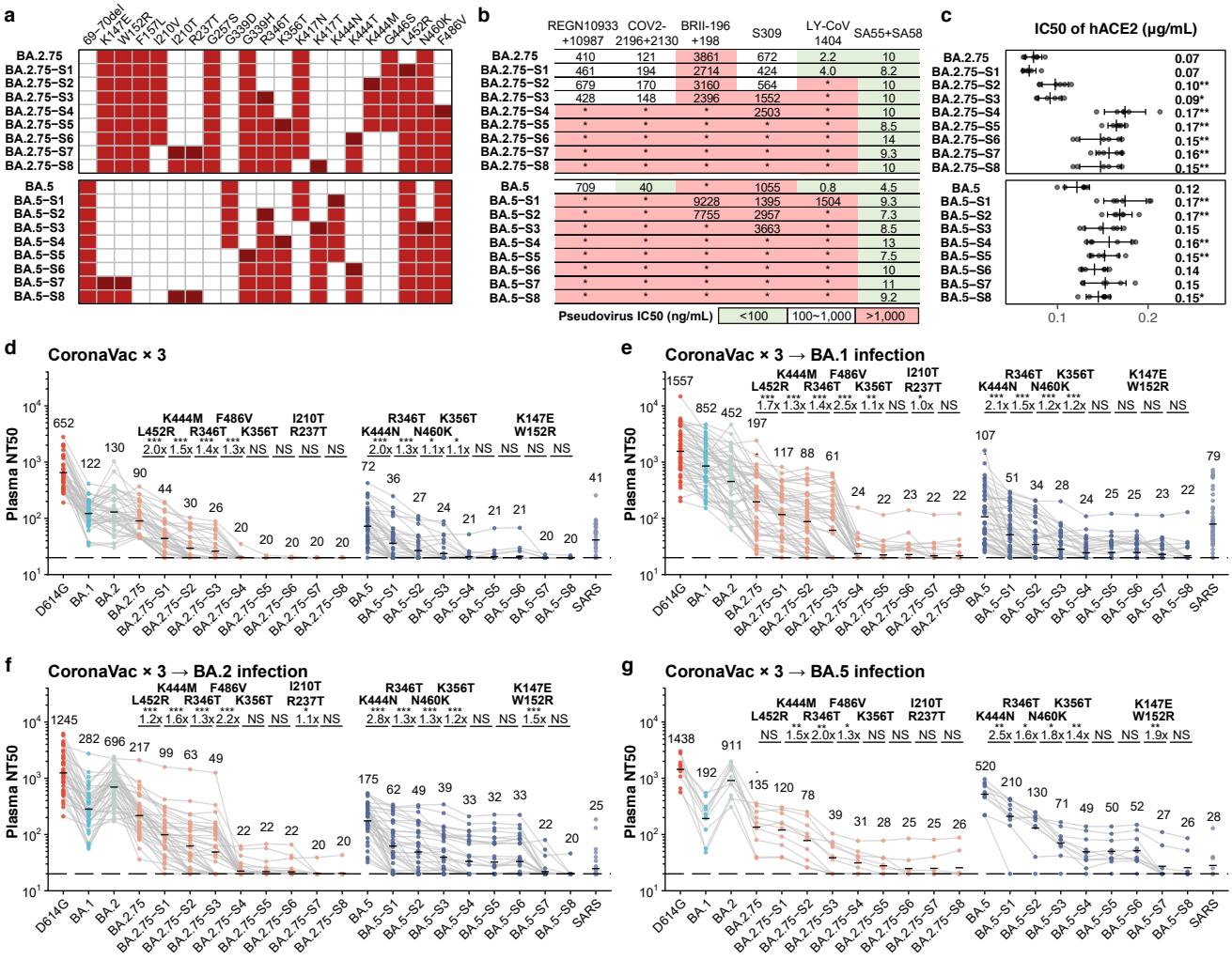

Fig. 5 | Accumulation of convergent escape mutations leads to complete loss of neutralization.
a, Mutations of multiple designed mutants that harbors key convergent escape mutations based on BA.2.75 and BA.5. b, IC50 of therapeutic mAbs and cocktails against pseudoviruses of designed mutants. green, IC50 ≤ 100ng/mL; white, 100ng/mL < IC50 < 1,000ng/mL; red, IC50 ≥ 1,000ng/mL; *, IC50 ≥ 10,000ng/mL. c, IC50 of hACE2 against the designed mutants. Error bars indicate mean±s.d. P-values were calculated using two-tailed Wilcoxon's rank-sum test. *, $p < 0.05$; **, $p < 0.01$; ***, $p < 0.001$. No label on variants with $p > 0.05$. d-g, Pseudovirus neutralizing titres against SARS-CoV-2 D614G, Omicron subvariants and designed mutants of plasma from vaccinated or convalescent individuals from breakthrough infection. d, Individuals who received 3 doses of CoronaVac (n = 40). e, Convalescents infected with BA.1 after receiving 3 doses of CoronaVac (n = 50). f, Convalescents infected with BA.2 after receiving 3 doses of CoronaVac (n = 39). g, Convalescents infected with BA.5 after receiving 3 doses of CoronaVac (n = 10). Key additional mutations harbored by each designed mutant are annotated above the points. The geometric mean titers are labeled. P-values are determined using two-tailed Wilcoxon signed-rank tests of paired samples. *, $p < 0.05$; **, $p < 0.01$; ***, $p < 0.001$; NS, not significant, $p > 0.05$. Statistical test are determined using two-tailed Wilcoxon signed-rank tests.

Extended Data Fig 1

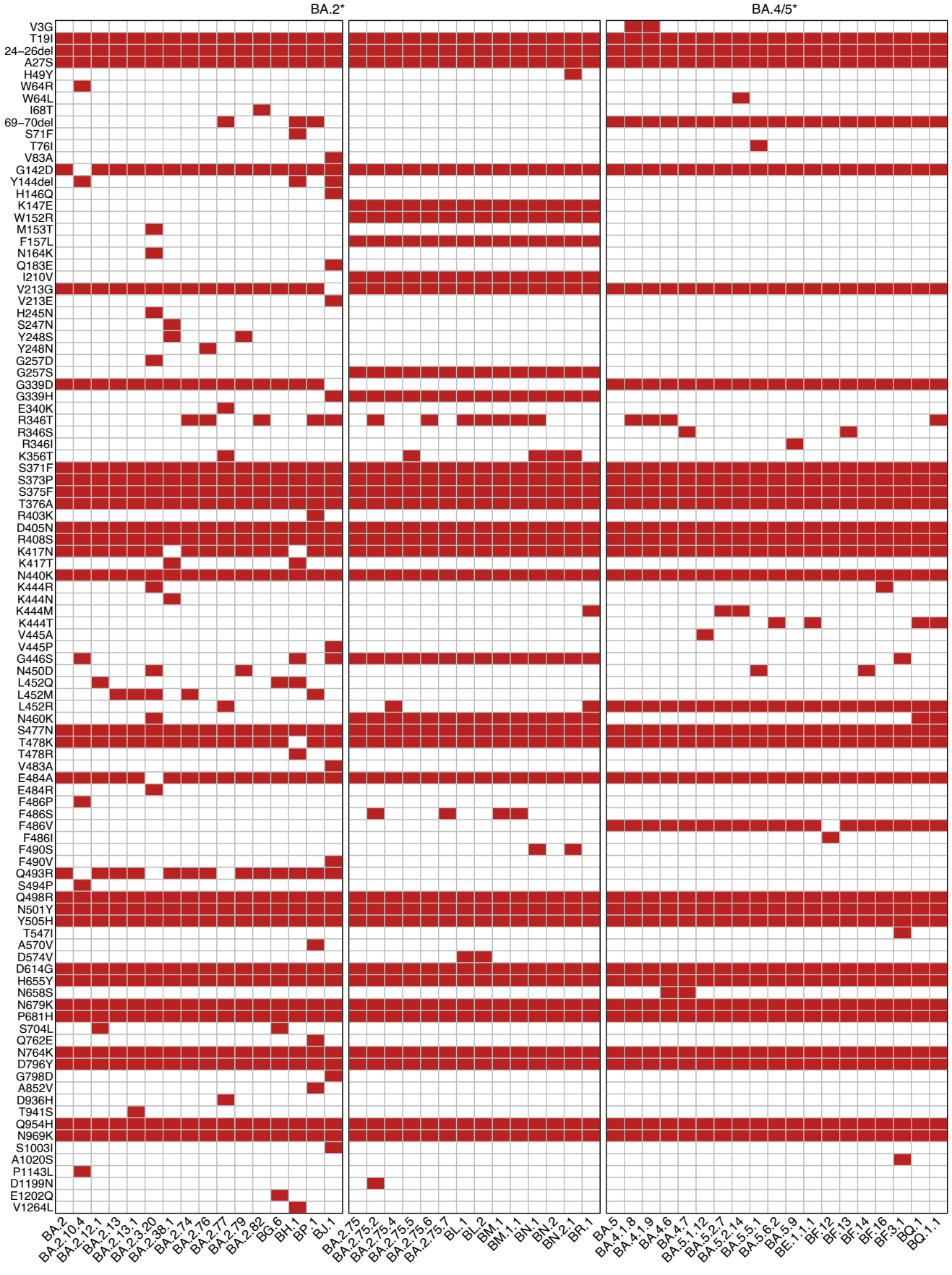

Extended Data Fig 2

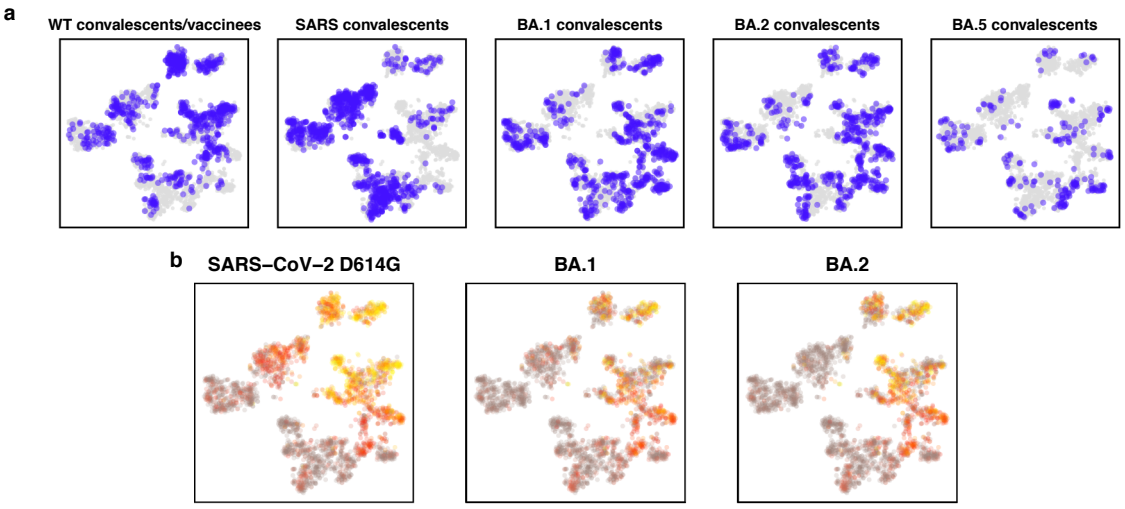

Extended Data Fig 3

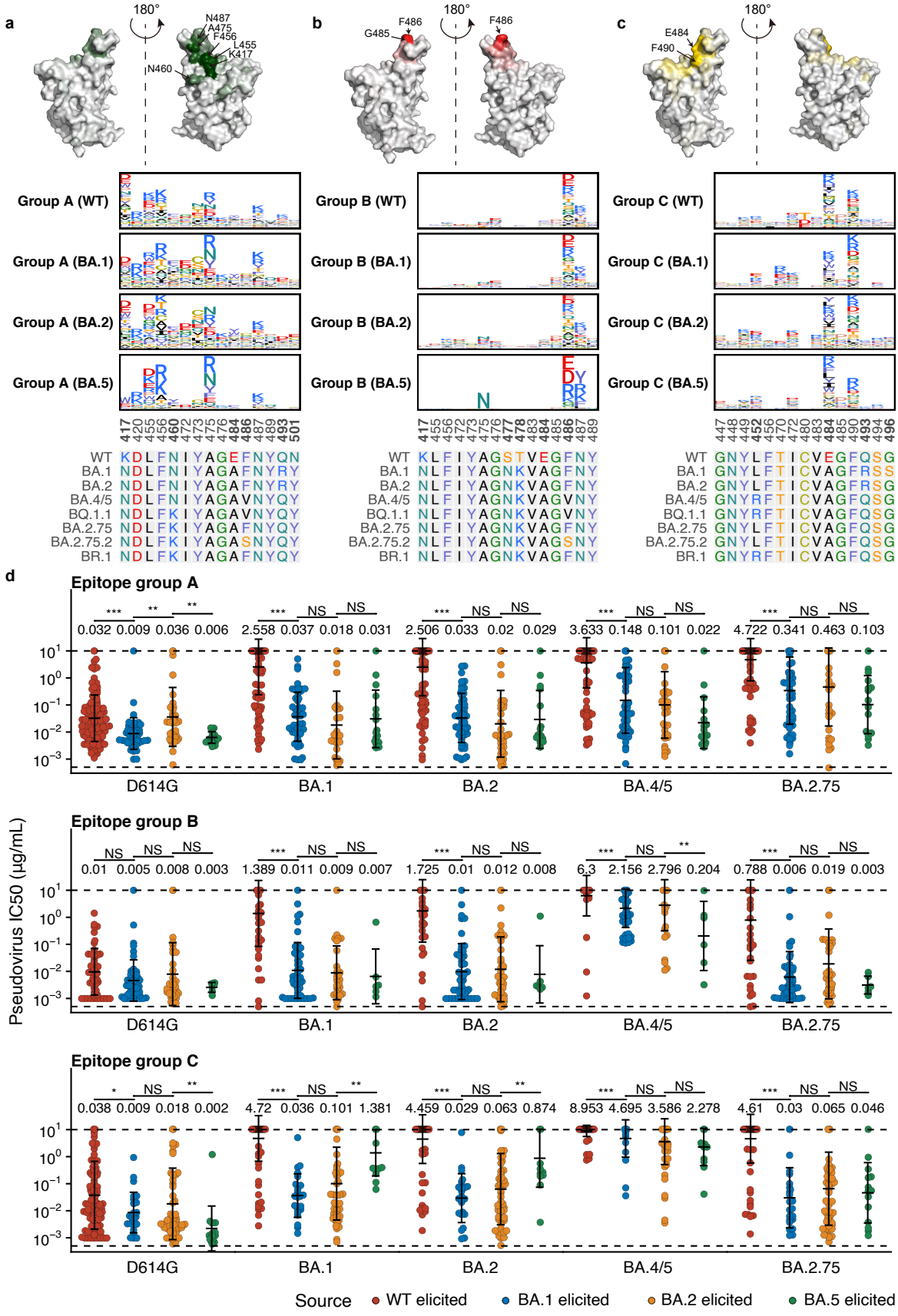

Extended Data Fig 4

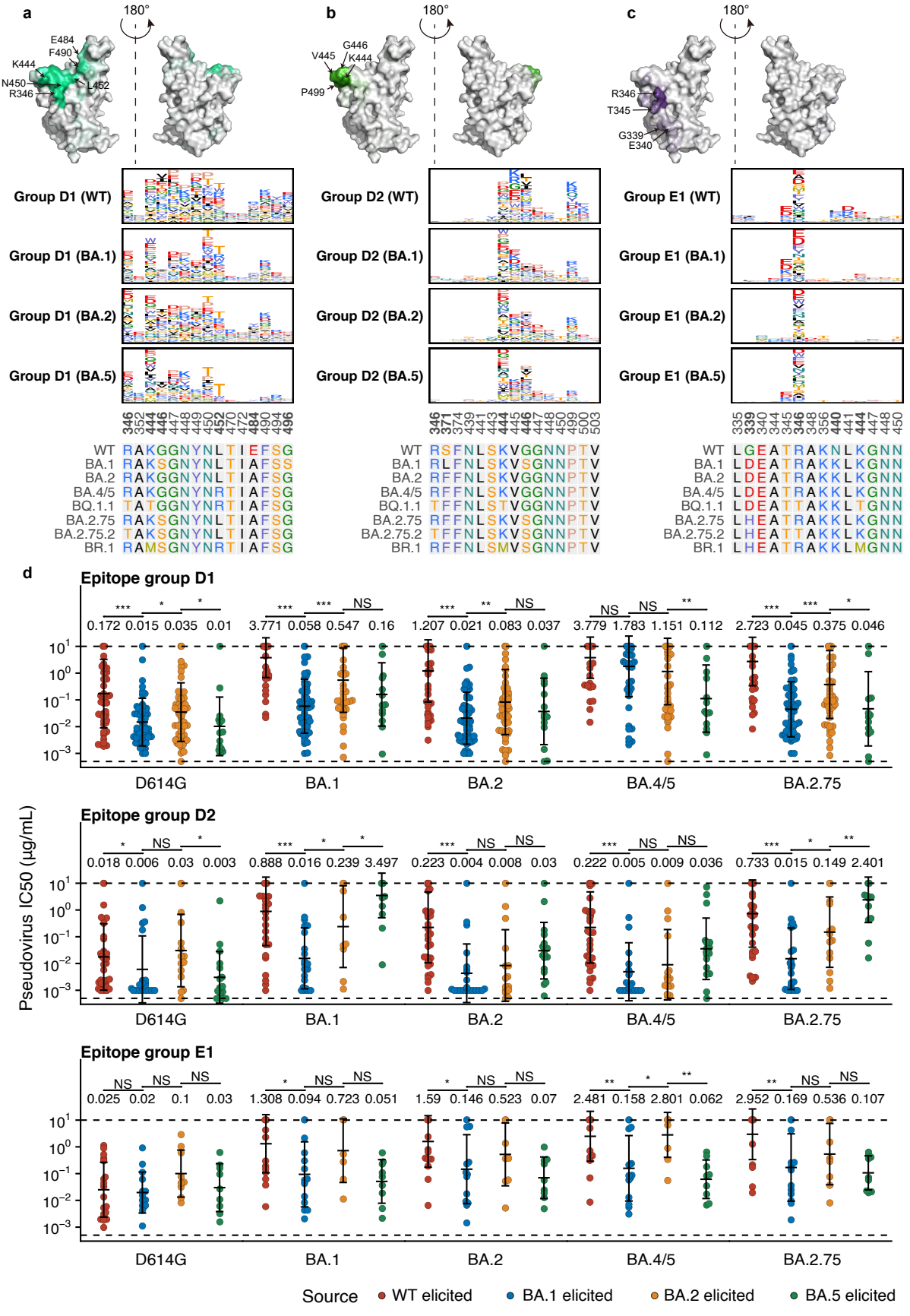

Extended Data Fig 5

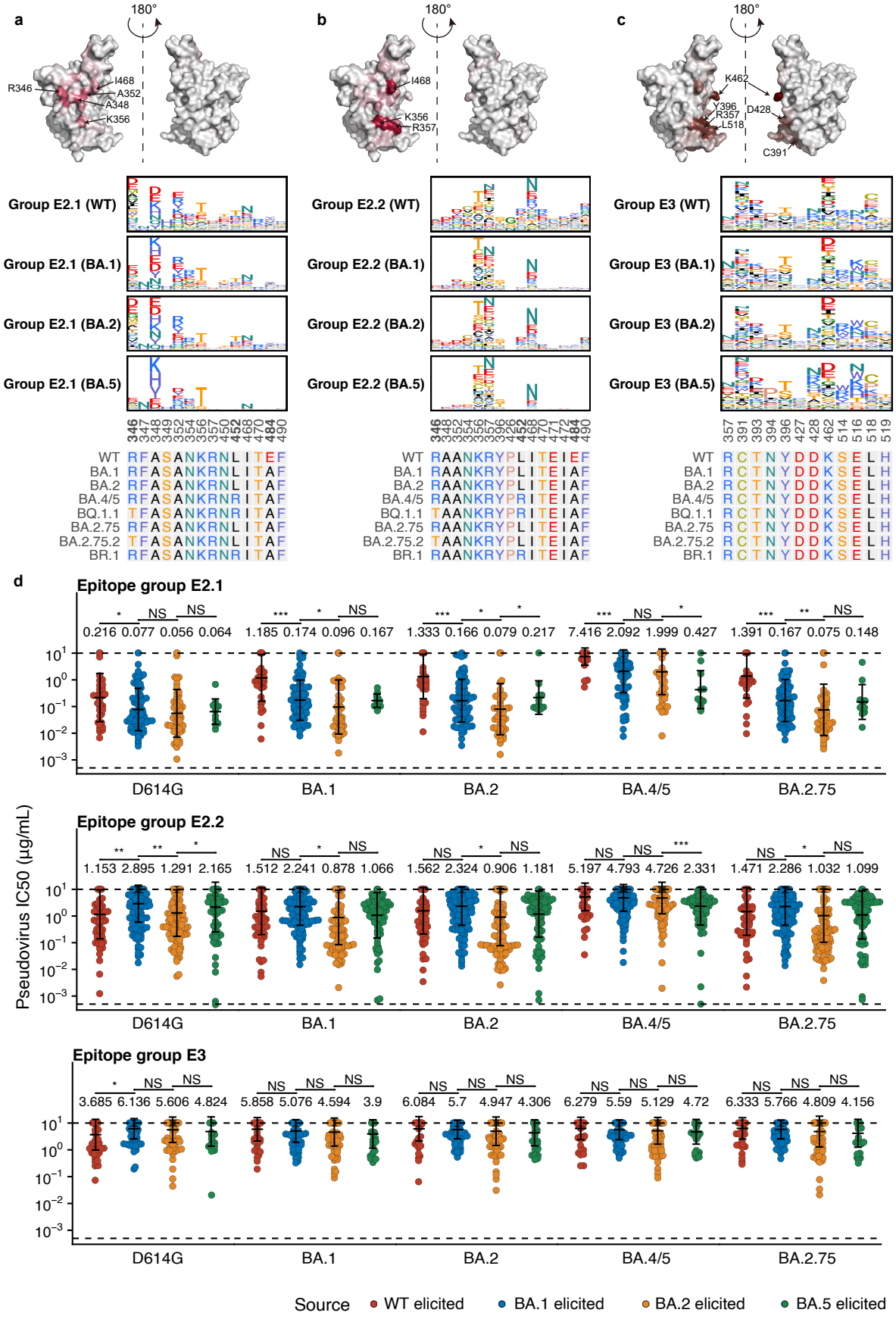

Extended Data Fig 6

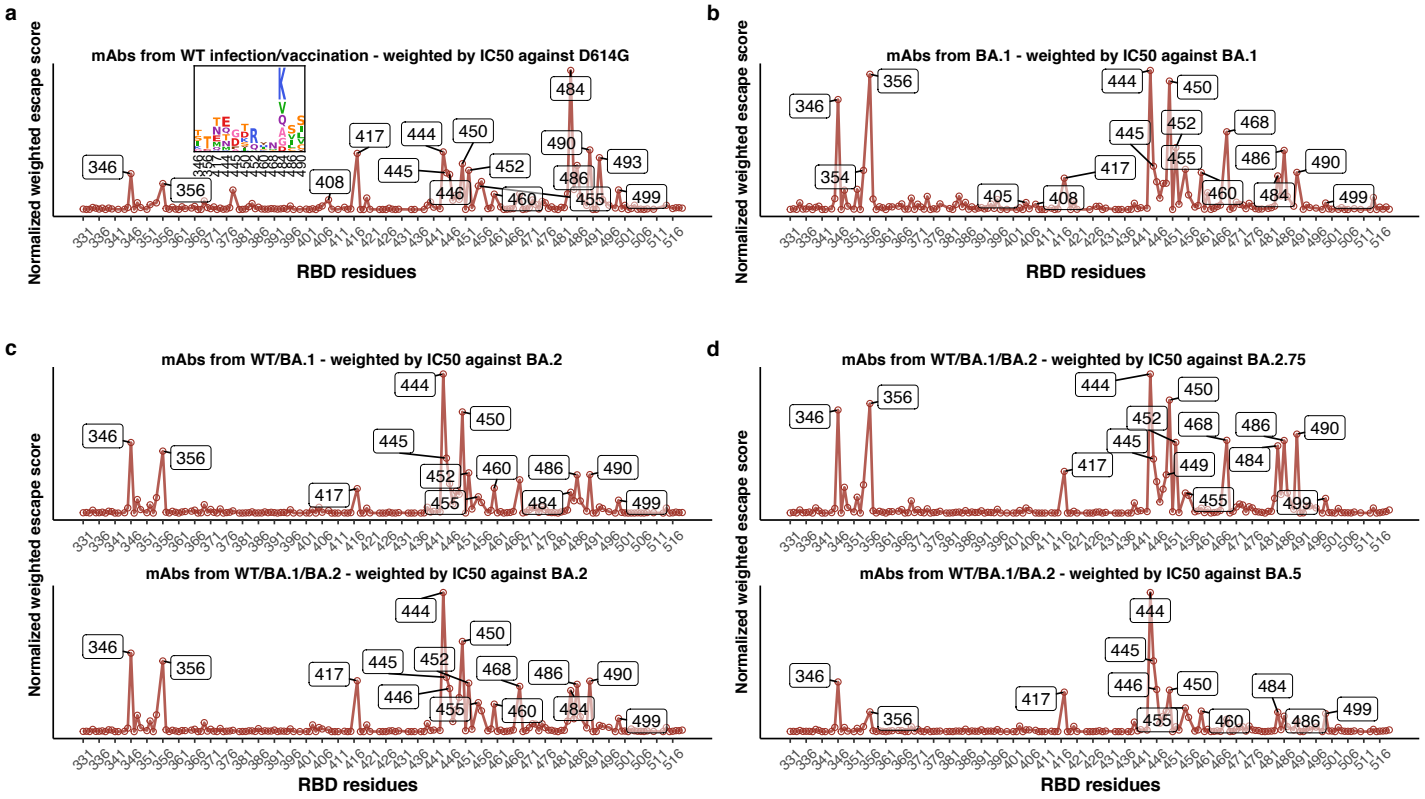

Extended Data Fig 7